A&A 560, A49 (2013)
DOI: 10.1051/0004-6361/201220627

Astronomy & Astrophysics

An archive study of 18 old novae

I. The UV spectra⋆,⋆⋆,⋆⋆⋆

P. Selvelli[1] and R. Gilmozzi[2]

[1] INAF – Ossservatorio Astronomico di Trieste, via Tiepolo 11, 34143 Trieste, Italy
e-mail: selvelli@oats.inaf.it
[2] European Southern Observatory, Karl Schwarzschild-Str. 2, 85748 Garching, Germany
e-mail: rgilmozz@eso.org

Received 25 October 2012 / Accepted 14 September 2013

ABSTRACT

Aims. We present an overview of the UV spectral properties of old novae as a class. The data and results of this paper, together with data from the outburst phases, will be utilized in a follow-up study to determine statistical properties and to investigate correlations among the physical parameters of the quiescent and eruptive phases.
Methods. All the available IUE, HST, and FUSE archive data for 18 old novae were used to derive accurate and homogeneous estimates of the reddening from the 2175 Å extinction bump and to determine the intrinsic spectral energy distribution corresponding to the utilization of both existing extinction curves. We also measured all the emission and absorption lines.
Results. We have found good agreement between spectra taken at different epochs and by different instruments, a clear indication of the near constancy of the SED on timescales of several years. With the possible exception of GK Per, the dereddened UV continua are represented well by a single-curve power-law distribution $F_\lambda \propto \lambda^{-\alpha}$, with α in the range 0.32–2.55 for one curve and 0.35–2.88 for the other one. The extrapolation of the various UV power laws to the optical range yields values that are in good agreement with the V magnitudes. We interpret this result as evidence that the SED is dominated by the accretion disk in the UV and optical spectral regions. A detailed study of the emission spectrum has led to measuring and identifying more than one hundred features and to detecting several lines that are rather uncommon in other CVs and whose identification is uncertain.

Key words. novae, cataclysmic variables – ultraviolet: stars – line: identification

1. Introduction

Old novae represent the (nearly) quiescent stage of a system that has undergone a historical classical nova explosion (outburst). Classical novae are members of the class of cataclysmic variables (CVs), i.e., semi-detached binary systems with $P \sim$ hours, in which hydrogen-rich material is transferred, through the inner Lagrangian point, from a Roche-lobe-filling, low main sequence star onto the surface of the primary white dwarf via an accretion disk.

Theoretical models for the outburst of classical novae require low accretion rates during quiescence (10^{-9} to 10^{-10} $M_\odot$ yr^{-1}) (Shara 1989). Only at these rather low rates does the material at the bottom of the H-rich envelope remain degenerate enough to ensure the strong observed flash when the critical ignition pressure is reached. Instead, the available observations of "historical" old novae generally indicate a rather high luminosity that, when interpreted in the framework of current accretion models, implies accretion rates between 10^{-9} $M_\odot$ yr^{-1} and 10^{-8} $M_\odot$ yr^{-1}.

This apparent disagreement between the theoretically required and the observed mass accretion rates is a rather disturbing problem in our understanding of the classical nova phenomenon. Theorists have proposed several possible solutions to this apparent contradiction (see Shara et al. 1986; Kovetz et al. 1987; Livio 1988). It should be pointed out, however, that any reliable statements about the "observed" $\dot{M}$ can only be obtained by observations that cover the UV range since the bulk of the accretion luminosity is emitted in this spectral region (Wade & Hubeny 1998; Orosz & Wade 2003; see also Paper II).

Unlike dwarf novae, which alternate low and high states, old novae (with the exception of GK Per and possibly V446 Her) are nearly steady accretors. This offers the opportunity to compare the energy distribution of "real" accretion disks with the expectations of the "standard" (steady) disk model ($F(\lambda) \propto \lambda^{-2.33}$) (Franck et al. 2002) or with those of specific accretion disk models (Wade & Hubeny 1998). Previous UV-based studies of novae during quiescent phases have focused on the individual behavior of the brightest members (see Krautter et al. 1981; Friedjung et al. 1982; Rosino et al. 1982; Bianchini & Sabbadin 1983; Selvelli et al. 1998; Borczyk et al. 2003; Moyer et al. 2003; Selvelli & Friedjung 2004; Engle & Sion 2005; Kolobow & Sion 2011).

While detailed studies of individual systems are essential, it is also important to complement these studies with an overview of the collective UV properties of these objects as a class. In this respect it is worth pointing out that, in contrast to the large number of UV (mostly IUE) and far-UV (mostly FUSE) studies for other classes of CVs (see, for example, Verbunt & Wade 1984; La Dous 1991; Mauche et al. 1997; Araujo-Betancor et al. 2005; Long 2006; Gänsicke et al. 2006; Hamilton et al. 2007; Sion et al. 2008; Froning et al. 2012), in the case of old novae,

⋆ Based on INES data from the IUE satellite. Some of the data presented in this paper were obtained from the Multimission Archive at the Space Telescope Science Institute (MAST).
⋆⋆ Tables 2–7 and 10–14 are available in electronic form at http://www.aanda.org
⋆⋆⋆ The final reduced spectra (FITS files) and full Table 2 are only available at the CDS via anonymous ftp to cdsarc.u-strasbg.fr (130.79.128.5) or via http://cdsarc.u-strasbg.fr/viz-bin/qcat?J/A+A/560/A49

the studies have been fairly preliminary (Gilmozzi et al. 1994; Selvelli 2004) or limited to a subset of objects (Szkody et al. 1991; Puebla et al. 2007, 2011).

To fill this gap, we present here (Paper I) the results of a study of the UV continuum energy distribution and the UV line spectrum of 18 old novae, based mostly on IUE but also on HST-FOS, HST-GHRS, HST-STIS, and FUSE observations, complemented by data on the optical magnitudes. In a follow-up study (Paper II), we will combine the main results of this paper with other data for both the quiescent and outburst phases to derive collective properties for the objects in this sample and to investigate the correlations among the physical parameters during both quiescence and outburst.

2. The UV data and their reduction

By mining the IUE and the MAST archives, we have found UV spectra belonging to twenty old novae, the vast majority from IUE (Boggess et al. 1978), complemented for some objects by data, generally unpublished, which was obtained with HST-GHRS, HST-STIS, HST-FOS. and FUSE. The spectra of recurrent novae in quiescent phase have not been included here for the sake of homogeneity.

2.1. IUE

All the available IUE files containing the extracted spectrum and the resampled image (SILO) have been retrieved from the IUE-INES archive and carefully inspected for their quality. For several objects, the observations were at the limit of the IUE capabilities: only five objects (i.e., V603 Aql, HR Del, RR Pic, GK per, V841 Oph) are relatively bright ($m_V \sim 11$–13), while the others have $m_V \geq 14$, up to $m_V = 17$, see also Table 9.

X Ser was excluded from the sample because of the signal-to-noise ratio that was too low in all the spectra. Nova Sgr 1962 has also been excluded because it was, quite surprisingly, still in a post-nova (nebular-like) stage at the time of the IUE observations. Table 1 gives the final list and basic information for the eighteen selected objects.

Some individual spectra of faint objects (e.g., LWP02268, LWR13902, SWP17635, SWP17636, SWP21544, SWP21545, SWP21546 (T Aur), SWP48292, SWP48538 (DK Lac), SWP25446, SWP54222, LWP05516 (BT Mon), and SWP07083 (V533 Her)) are very noisy and have also been disregarded. For GK Per, which undergoes dwarf-nova-like outbursts with a recurrence time of about 1000 days, we only used pairs of SW and LW spectra taken in sequence when the star was in a low state. For V446 Her, we disregarded the two available IUE spectra and instead utilized the STIS spectra that have a higher signal, especially in the $\lambda\lambda$ 2000–2400 Å region, which is critical for the reddening correction.

Tables 2 gives an excerpt of the list of IUE spectra of bright old novae (full list available at the CDS), while Table 3 gives the list of all IUE spectra of faint old novae that were used. With the only exception of BT Mon (see the following), they were retrieved from the INES final archive, based on the IUE Newly Extracted Spectra system developed at the European Space Agency (ESA) IUE Ground Station of Villafranca del Castillo (Madrid, Spain). For a detailed description of the IUE-INES system see Rodriguez-Pascual et al. (1999) and González-Riestra et al. (2001).

The most relevant modifications in the INES system, in comparison with the NEWSIPS system (adopted in the HST-MAST and NASA archives) are 1) the adoption of a new noise model; 2) a more accurate representation of the spatial profile of the spectrum; 3) a more reliable determination of the background; 4) a more adequate treatment of "bad" pixels; and 5) improvement in the handling and propagation of the quality flags to the final extracted spectra. In general, for "normal" stars, the extracted fluxes of INES and NEWSIPS are in excellent agreement, but in the case of spectra with weak continua and narrow emission lines, the INES extraction generally registers significantly more flux (Schartel & Skillen 1998). Therefore, the INES extraction procedure has led to general improvement in the quality of the line spectrum for objects with weak continuum and rather sharp emission lines, that is, for conditions that are generally encountered in the spectra of the faintest old novae. The only exception we have found to this general trend is for the two spectra of BT Mon (SWP27732 and LWP07668), whose NEWSIPS extraction gives a higher signal-to-noise ratio (S/N), and has therefore been adopted.

Another important difference between the INES and NEWSIPS data reduction methods is in the treatment of the emission knots (spikes) located outside the strip that defines the spectrum. They are generally flagged as "cosmic rays" but in some cases they may be real spectral features originating in an extended region. (This is especially valid for an old nova with a surrounding nebula.) While NEWSIPS automatically removes these lines (with the risk of also removing real emission features), INES is more conservative and keeps the features but puts a proper quality flag in the corresponding spectrum column. In view of these problems that are especially critical when dealing with the spectrum of an object that could be surrounded by an extended shell, we have carefully checked all spectral images (SILO) in order to guarantee the reality of the emission features that are present in the INES extracted spectra (see also Sect. 6).

For the brightest objects (e.g., V603 Aql, RR Pic, HR Del, GK Per) for which several spectra are available, it is immediately clear that the individual spectra are very similar, since the UV continuum intensity and slope are nearly constant, with only minor variations on the order of 10%. Since the study of the small short-time variations of the continuum and lines in individual objects is beyond the scope of the present study

Table 1. Coordinates (J2000), orbital periods in days (Ritter & Kolb 2010), and year of the outburst for the 18 old novae under study.

Object	α	δ	P_d	Year
V603 Aql	18 48 54.64	+00 35 02.9	0.138	1918
T Aur	05 31 59.12	+30 26 45.0	0.204	1891
Q Cyg	21 41 43.92	+42 50 29.1	0.420	1876
HR Del	20 42 20.35	+19 09 39.3	0.214	1967
DN Gem	06 54 54.35	+32 08 28.0	0.128	1912
DQ Her	18 07 30.25	+45 51 32.6	0.194	1934
V446 Her	18 57 21.51	+13 14 29.9	0.207	1960
V533 Her	18 14 20.48	+41 51 22.1	0.148	1963
CP Lac	22 15 41.09	+55 37 01.4	0.145	1936
DI Lac	22 35 48.48	+52 42 59.7	0.544	1910
DK Lac	22 49 46.91	+53 17 19.3	0.130	1950
HR Lyr	18 53 25.05	+29 13 37.7	0.1:	1919
BT Mon	06 43 47.24	–02 01 13.9	0.339	1939
GI Mon	07 26 47.11	–06 40 29.8	0.180	1918
V841 Oph	16 59 30.37	–12 53 27.1	0.601	1848
GK Per	03 31 11.82	+43 54 16.8	1.997	1901
RR Pic	06 35 36.06	–62 38 24.3	0.145	1925
CP Pup	08 11 46.06	–35 21 04.9	0.061	1942

(see the papers by Friedjung et al. 1997; Silber et al. 1996; Selvelli et al. 1998; Prinja et al. 2000; Borczyk et al. 2003; Selvelli & Friedjung 2004), for the objects mentioned above we have created a low-noise, average spectrum by co-adding and merging all the far-UV ($\lambda\lambda$ 1200–1980 Å, SWP region) and near-UV ($\lambda\lambda$ 1980–3200 Å, LWR/LWP region) individual spectra that are not underexposed or badly centered (see Figs. 1, 2, 7, and 8, to appreciate the high quality of the IUE-averaged spectra of V603 Aql and RR Pic). This has allow detection of weak spectral lines and more precise estimates of the E_{B-V} correction and of the continuum slope.

For the faint objects, the IUE observations were at the limit of the instrument capabilities and, in spite of the long exposure times, the spectra of BT Mon, CP Lac, CP Pup, DK Lac, and HR Lyr are generally quite noisy, especially in the $\lambda\lambda$ 2000–2400 Å region. This is an unfortunate combination of the intrinsic low sensitivity of the IUE LW camera in this wavelength region, coupled to the intrinsic decrease in the observed flux as a consequence of the wide IS absorption bump centered on λ 2200 Å.

2.2. HST-FOS

HST-FOS observations were secured for only two objects of our sample of old novae: V603 Aql and DQ Her. The corresponding datasets with good data quality have been retrieved from the MAST databank (Table 4).

For V603 Aql, two spectra were taken with the G160 grating and one spectrum with a prism, all in the RAPID mode. Each dataset contains about 1000 independent subintegrations that were intended for a study of short-time spectral variations. In the present study, which deals with the average spectral behavior and requires good quality data, each group of short-time subexposures has been averaged into an individual spectrum, and the individual spectra have been merged into a single spectrum covering the wavelength range from 1200 Å to about 9000 Å using standard IRAF[1] routines (strfits, rcombine, mkmultispec, scombine): see also Fig. 1.

For DQ Her, the number of secured FOS spectra is much higher (see Table 4) and, as in the case of above, each dataset contains independent subintegrations. These observations allowed a study of pulsations and short-time variations (see Silber et al. 1996a,b). For our purposes here, again, each group of short-time subexposures (with the exclusion of the few spectra taken during eclipse) has been averaged into an individual spectrum, and these spectra have been merged into a single average spectrum with higher S/N: see also Fig. 3.

2.3. HST-GHRS

HST-GHRS observations are available only for V603 Aql and were secured at two different epochs. Table 5 gives the datasets containing good quality data. As in the case of the FOS data, each observation (dataset) contains many (about 1000) independent sub-integrations. These observations were intended for a study of short-time spectral variations (see Prinja et al. 2000; Friedjung et al. 1997). In the present study, for the reasons outlined in the previous section, each group of short-time subexposures was averaged into an individual spectrum, and the individual spectra were merged into a single spectrum covering the wavelength range $\lambda\lambda$ 1180–1670 Å and employing standard IRAF routines as in the case of the FOS data. See also Fig. 1.

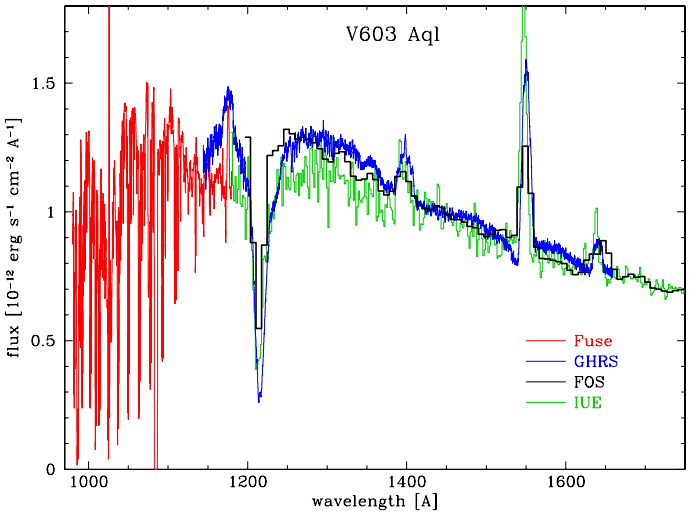

Fig. 1. Portion of the far-UV spectrum of V603 Aql with data from FUSE, FOS, IUE, and GHRS. The IUE spectrum is a grand average from about 100 individual spectra. Several weak features not detectable in individual spectra have emerged. See Tables 10–12 for line identification.

2.4. HST-STIS

HST-STIS spectral data for V446 Her, T Aur, and DI Lac were retrieved from the MAST archive (Table 6). The G140L first-order grating and the E140M echelle grating cover the spectral range 1150–1720 Å, while the G230L grating covers the range $\lambda\lambda$ 1570–3180 Å. The spectral data were reduced using standard IRAF routines (tomultispec, wfits, scopy, scombine). In the case of V446 Her, for which pairs of far-UV and near-UV data are available, the far-UV and near-UV spectra were averaged and merged into a single high-quality spectrum that covers the range 1160–3160 Å. The agreement between the IUE and STIS data of V446 Her is quite good in the near-UV but rather coarse toward shorter wavelengths, a consequence of the low quality of the IUE data in this spectral range. For this reason, in the case of V446 Her, we utilized only the STIS spectrum for the estimate of the reddening and for the measurements of the continuum and line intensities. For T Aur and DI Lac (Moyer et al. 2003), only far-UV data ($\lambda\lambda$ 1200–1700 Å) are available and have been used for comparison with the IUE and the FUSE data (see Figs. 4 and 6) and for measurements of lines.

2.5. FUSE

Spectroscopic data of five old novae, V603 Aql, V533 Her, DQ Her, RR Pic, and DI Lac, are present in the FUSE archive (see Table 7), although to the best of our knowledge, only the FUSE data of DQ Her have been utilized, so far, in a research paper (Froning et al. 2012). All spectra were taken using the LWRS aperture and in "time-tag" observing mode.

We refer to the FUSE Data Analysis Cookbook (Sankrit & Anderson 2005) for details about the FUSE observations and the reading of the data. The above-mentioned paper by Froning et al. (2012) also contains useful and detailed descriptions of

[1] IRAF is distributed by the National Optical Astronomy Observatory, Tucson, AZ, USA, which is operated by the Association of Universities for Research in Astronomy (AURA) under cooperative agreement with the National Science Foundation.

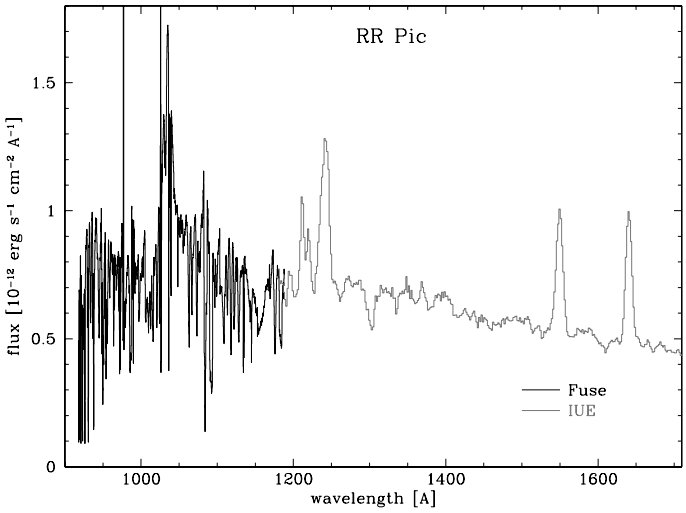

Fig. 2. Portion of the far-UV spectrum of RR Pic with data from FUSE and IUE. The IUE spectrum is an average from 23 individual spectra. Several weak features not detectable in individual spectra have emerged. See Tables 10–12 for line identification.

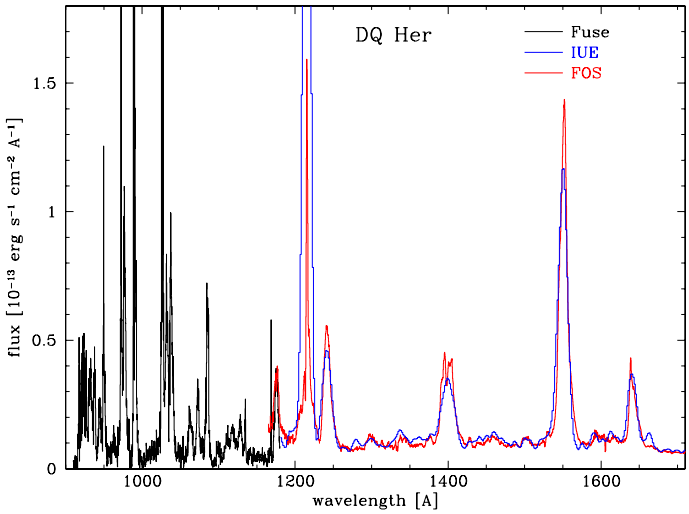

Fig. 3. Portion of the far-UV spectrum of DQ Her with data from FUSE, HST-FOS, and IUE. The strong emission near λ 1215 Å in the IUE spectrum is mainly geo-coronal Lyman-alpha. See Tables 10–12 for line identification.

the various problems one encounters in reducing the FUSE data. The processing of the FUSE spectra is not a straightforward operation owing to the way the data are acquired. A given FUSE observation is generally made up of a set of multiple exposures, and each exposure consists of data taken on four independent detector segments: 1A, 1B, 2A, 2B. In turn, each segment has two channels, LiF (lithium fluoride) and SiC (silicon carbide), so that for each observation, eight independent spectral segments are produced. Flux from individual exposures are added together to get the final spectrum. There are, however, several problems that affect the process of adding individual spectra:

1. the location of the target within the aperture can differ from one exposure to the next;
2. jitter in the spacecraft moves the target around;
3. channel drift: the FUSE optical bench flexes slightly on orbital timescales, causing the line of sight of the primary mirror to shift by several arcseconds from one orbit to another. Therefore the source could move in and out of the aperture during an exposure: counts are lost, the true exposure time is lower that the commanded exposure time, and the calculated flux is underestimated.

In the present study, for each object and each observation, this has required a careful and detailed examination of the individual spectra before the data were combined. In several cases, individual spectra were disregarded because of high noise level. Using IRAF routines (tabim, mkmultispec, scombine, scopy), the eight individual spectral segments for each observation were combined to create a single time-averaged broad-band spectrum that covers the full FUSE wavelength range $\lambda\,\lambda$ 905–1187 Å.

In the case of V603 Aql, the data of the SiC channels are quite poor and have been disregarded. In the case of RR Pic, all individual spectra from the dataset S7011202000 and a few from the other datasets have also been disregarded because of their low S/N quality. For RR Pic, since there were no substantial changes in spectra from different observations, they were combined into a single spectrum to improve S/N. All FUSE final spectra have been moderately smoothed with a Gaussian convolution, which is a routine of the iraf guiapps-spectool external application. See also Fig. 2.

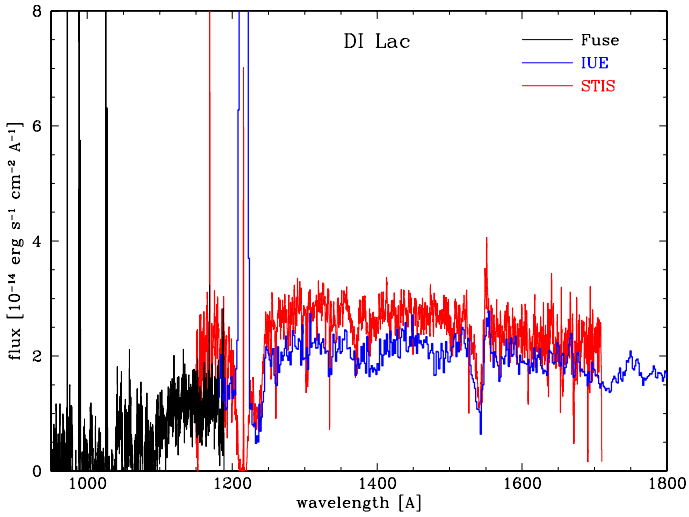

Fig. 4. Portion of the far-UV spectrum of DI Lac with data from FUSE, STIS and IUE. See Tables 10 and 11 for line identification.

3. The near constancy of the UV flux

For the seven objects for which UV spectra other than IUE are available, the comparison of portions of spectra taken with different instruments and at different epochs shows (with the partial exception of V446 Her) a good agreement between the various spectral portions and/or overlaps; see Figs. 1 through 6. Orio et al. (2009) also note that for CP Pup there was no evidence of flux change in the common wavelength range covered by the IUE-LWP camera and by the UV filters of the *XMM-Newton* OM between 1986 and 2005. This near constancy is remarkable, on account of the variability with different timescales generally observed in old novae and associated to various mechanisms, such as rotation, orbital motions, hot spots, instabilities and inhomogeneities in the accretion disk, cycles of activity in the secondary (Bianchini 1990), and is clear evidence of both the near constancy of the average flux over years and the high quality of the calibrations for the different instruments.

It is clear that, since the UV observations span only a time interval of about 15–20 years, the observed near constancy of the

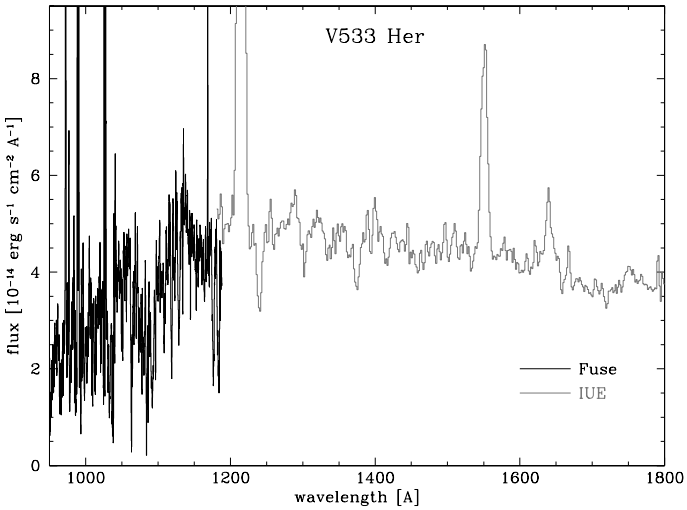

Fig. 5. Portion of the far-UV spectrum of V533 Her with data from FUSE and IUE. The strong Lyα emission in the IUE range is mostly geo-coronal. The sharp emission lines in the FUSE range are due to geo- and helio-coronal contamination. See Tables 10 and 11 for line identification.

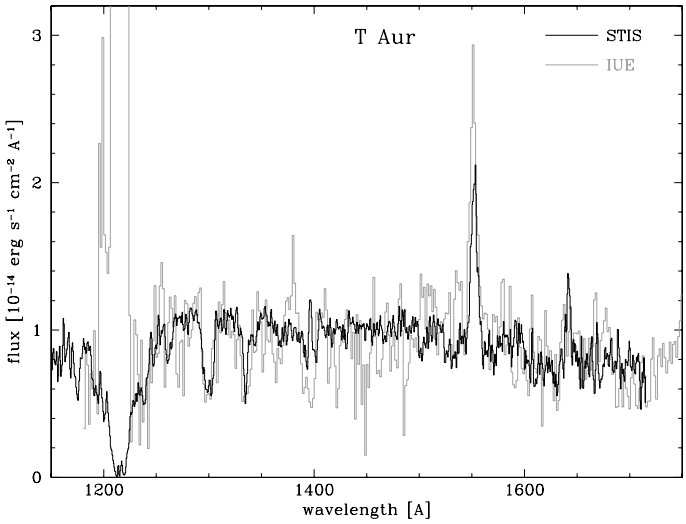

Fig. 6. Portion of the far-UV spectrum of T Aurigae with data from HST-STIS and IUE. The strong emission line near λ 1215 in the IUE spectrum is the geo-coronal Lyman-alpha. See Tables 10 and 11 for line identification.

UV flux for each single object only refers to this small fraction of time in the evolution of the system after outburst. However, that near constancy in the UV flux is observed in objects with a wide range in the time elapsed from the outburst, from a minimum of about 20 years for HR Del to a maximum of about 130 years for V841 Oph (see Table 1) seems to indicate near constancy in the UV flux over a longer time interval. Needless to say, new UV observations are required to confirm this indication, in particular for the objects in our sample for which only one single UV spectrum is available.

Most old novae are also known to undergo short-time variations (flickering); however, the exposure times of the integrated HST-FOS HST-GHRS HST-STIS, and FUSE spectra are quite long and comparable to those of the IUE spectra. Therefore, in all cases the comparison is quite homogeneous, that is, between spectra where most of the short time variations are smoothed out.

The near constancy of the average UV flux at different epochs clearly indicates a near constancy of the mass accretion rate. We postpone to Paper II a detailed discussion concerning this fundamental parameter.

4. The reddening correction

Needless to say, an accurate estimate of the reddening correction is a very critical prerequisite for determining the accretion luminosity (and the mass accretion rate) because the correction affects the determination of *both* the intrinsic SED and the distance. In stellar studies, the extinction E_{B-V} is best determined using the standard "pair" method (Massa et al. 1983), i.e., comparison of the fluxes from two stars with nearly identical spectroscopic features but with one of the stars nearly unaffected by dust absorption. Neither this method nor the method of continuum fitting with stellar atmosphere models can be applied to old novae to determine extinction because of the lack of any reference standard, and because models are still quite rudimentary. Another method employs ratios of recombination lines or of emission lines arising from a common upper level (see for example Selvelli et al. 2007), but this is not applicable in our spectra on account of the lack of suitable emission lines.

However, the UV range is the one most sensitive to the effects of the presence of reddening, since it is characterized by the presence of a broad interstellar (IS) absorption bump in the SED curve, centered near λ 2175 Å. This can help us correct the observed distribution: for each suitable reddening law (Seaton 1979; Savage & Mathis 1979, hereinafter SM; Cardelli et al. 1989a,b, both together referred to as CCM hereinafter; Fitzpatrick 1999), the best estimate of E_{B-V} is the one that makes the extinction bump disappear completely.

In this work we have assumed that the intrinsic SED is represented by a power law $F_\lambda \sim \lambda^{-\alpha}$, and employing the method of "nulling" the 2175 bump, we have found the E_{B-V} value for which the resulting UV distribution is best represented by some power law.

The spectra were dereddened in steps of 0.02 mag in E_{B-V}, and the choice of the final E_{B-V} has been that of the intermediate value between those where a weak absorption bump or a weak emission bump was still appreciable. The latter values have been taken to define the accuracy of the color excess determination.

Some degree of uncertainty in this procedure is introduced by the fact that the IUE LW cameras have low sensitivity in the 2000–2400 range, as is evident from the high noise level at these wavelengths. However, the SWP camera has very high sensitivity up to 2000 Å, and the LW cameras have an increasing sensitivity longward of 2400 Å. Therefore the reddening can be estimated by imposing the plausible condition that the extension of the SWP and LW dereddened continua overlap in the noisy region.

It should be pointed out that the assumption of a power-law continuum distribution is justified on the observational side by the observed spectral distribution of old novae with low reddening, such as RR Pic, V533 Her, and V603 Aql. It is also justified on the theoretical side by the fact that the characteristic spectrum of a steady, optically thick accretion disk radiating locally as a black body is very close to that of a power-law distribution, with index –2.33 (Franck et al. 2002).

One complication in the procedure described above is that, as clearly pointed out by Fitzpatrick & Massa (2007), there appears to be no unique determination, or even a best estimate, for the mean Galactic extinction curve. The various extinction

Table 8. Reddening.

Object	(2)	(3)	(4)	(5)	(6)	(7)	(8)	(9)	(10)	(11)	(12)	(13)	(14)	(15)
V603 Aql	0.08 ± 0.02	0.16	0.16	0.08	0.07	0.07	0.08	0.07	0.07	0.07	0.08	0.82	5.02	2.33
T Aur	0.42 ± 0.08	0.40	0.40	0.39	0.62	–	0.39	0.38	0.21	0.21	0.39	–1.70	1.39	0.92
Q Cyg	0.26 ± 0.06	–	0.45	0.44	0.48	0.48	–	–	–	0.25	–	–7.55	0.45	0.45
HR Del	0.17 ± 0.02	0.18	0.18	0.15	0.17	0.17	0.15	0.07	0.15	0.15	0.15	–13.97	0.13	0.12
DN Gem	0.17 ± 0.04	0.09	0.09	0.08	0.13	–	–	–	–	0.10	0.13	14.71	0.10	0.18
DQ Her	0.05 ± 0.02	0.05	0.05	0.05	0.08	0.08	0.08	0.07	0.10	0.10	–	26.44	0.04	0.05
V446 Her	0.38 ± 0.04	0.55	–	–	0.55	–	–	0.26	0.36	0.36	–	4.70	0.93	0.70
V533 Her	0.03 ± 0.02	0.08	0.08	0.03	0.19	–	0.03	0.19	0.00	0.00	0.03	24.27	0.05	0.07
CP Lac	0.28 ± 0.06	0.48	–	–	0.48	0.47	–	0.26	0.21	0.20	–	–0.83	1.64	0.94
DI Lac	0.26 ± 0.04	–	0.42	0.41	0.41	0.41	0.41	–	–	0.16	0.41	–4.85	0.44	0.53
DK Lac	0.22 ± 0.06	0.39	–	–	0.45	0.45	–	0.45	0.45	0.44	–	–5.35	0.33	0.45
HR Lyr	0.18 ± 0.06	–	–	0.14	0.15	–	0.15	–	–	0.16	–	12.47	0.17	0.22
BT Mon	0.24 ± 0.06	0.20	0.20	–	–	–	–	–	0.16	0.15	0.15	–2.62	1.03	1.17
GI Mon	0.10 ± 0.04	–	–	–	–	–	–	–	–	–	–	4.75	0.20	0.45
V841 Oph	0.44 ± 0.06	–	0.40	0.39	0.58	0.58	0.39	–	–	0.32	0.39	17.77	0.45	0.25
GK Per	0.34 ± 0.04	0.23	–	0.29	0.10	0.29	0.29	0.10	0.31	0.30	–	–10.10	0.35	0.36
RR Pic	0.00 ± 0.02	0.01	0.01	0.02	–	–	0.02	0.06	0.05	0.05	0.02	–25.67	0.06	0.07
CP Pup	0.20 ± 0.04	0.26	–	0.25	–	–	0.25	0.09	0.25	0.25	0.21	–0.83	1.09	1.12

Notes. Columns 2 to 12 give the color excess E_{B-V} for the old novae in our sample, from this study and from the literature (see Notes). Column 13 gives the galactic latitude in degrees, Col. 14 gives the total galactic extinction from the reddening maps of Schlegel et al. (1998) using the NASA/IPAC extinction calculator, and Col. 15 gives the total galatic extinction from the neutral hydrogen maps (Kalberla et al. 2005) of the LAB survey, assuming an average gas to dust ratio $N_{\rm H}/E_{B-V} = 6 \pm 2 \times 10^{21}$ cm^{-2} mag^{-1} (Dickey & Lockman 1990).

References. (2) this work; (3) Duerbeck (1981); (4) Warner (1987); (5) Bruch & Engel (1994); (6) Weight et al. (1994); (7) Ringwald et al. (1996); (8) Diaz & Bruch (1997); (9) Shafter (1997); (10) Downes & Duerbeck (2000); (11) Downes & Duerbeck (2001); (12) Puebla et al. (2007).

curves mentioned above generally agree with one another longward of 1500 Å and therefore indicate a similar E_{B-V} correction from the bump, but at shorter wavelengths the CCM curve gives a higher correction compared to the curves of Seaton (1979) and SM, with the Fitzpatrick & Massa (2007) curve being intermediate. The consequence is that, for a given E_{B-V} there will be a non-negligible difference in the slope of the spectra shortward of 1500 Å for the different reddening curves with effects on the slope of the continuum on the estimated UV luminosity and, ultimately, on the mass accretion rate.

Therefore, to evaluate the effects of different reddening curves on these parameters, the UV spectra have been corrected using both the mean galactic extinction law of Savage & Mathis (1979) in the ESO-MIDAS[2] reduction package and the Cardelli et al. (1989a,b) extinction curve in the IRAF package.

We note that while the CCM curve has gained popularity, the SM curve has still been adopted in recent studies (e.g., Pottasch et al. 2013; Aidelman & Zorec 2012; Mc Elroy et al. 2013). Also, Sasseen et al. (2002) find that in the far-UV region the extinction curve is consistent with an extrapolation of the standard SM curve.

The color excess values E_{B-V} found in this study are given in Col. 2 of Table 8. They supersede the previous ones derived in our earlier studies (Gilmozzi et al. 1994; Selvelli 2004) that were based on a more limited number of stars and spectra. The E_{B-V} values are determined quite well for most objects, but uncertainties of ±0.06 mag are encountered in the spectra of T Aur Q Cyg, CP Lac, BT Mon, and DK Lac because of the rather high noise level in the region of the bump. For the brightest objects, for which many spectra are available, the uncertainty is about ±0.03 mag or less.

To provide a comparison with previous E_{B-V} determinations (and possibly as a service to the community), we have collected, in chronological order in the columns from (3) to (12) in Table 8, a list of various E_{B-V} values that are scattered in the literature. Our E_{B-V} values are in fair agreement with those of Duerbeck (1981) (with the exception of V603 Aql and DK Lac), those of Downes & Duerbeck (2001) (with the exception of T Aur and DK Lac), and, for the ten objects in common, with those by Puebla et al. (2007) (with the only exception of DI Lac). However, there are significant differences from the values given by Shafter (1997) and from those, generally higher, found by Weight (1994) and by Ringwald et al. (1996) in studies of the optical and IR spectra of cataclysmic variables. For GK Per, and based on the nova galactic coordinates,an estimate of the distance, and the dust prescription of Schlegel et al. (1988), Shara et al. (2012) derived $E(B-V) = 0.32$, a value very close to the one derived in this study.

We note that, with the exception of Puebla et al. (2007), most of the E_{B-V} values listed in Cols. 3–12 are not uniform, because they were obtained by various methods from the literature (e.g., Balmer decrement, IR maps, optical spectra, UV colors). In fact, the E_{B-V} values in this work represent the first homogeneous reddening determination for the old novae in the sample.

It turns out, but this is not a surprise, that objects at high galactic latitude (DQ Her, V533 Her, and RR Pic) have the lowest reddening values, see Table 8, Cols. 2 and 13. In Table 8, for reference, we have also included in Col. 14 the values of the total galactic extinction along the line of sight of the novae as determined by the galactic-reddening IR maps of IRAS and COBE/DIRBE as given by Schlegel et al. (1998). This method sets a reliable upper limit on the interstellar extinction E_{B-V} for the position of the novae. The "Dust Extinction Service"[3] uses the maps of Schlegel et al. to return the 100-micron intensity integrated along a line of sight through the Galaxy and corresponding estimates of the Galactic dust extinction. One can easily see that, as expected, the total galactic E values, with the

[2] http://www.eso.org/sci/software/esomidas/midas-distrib.html

[3] http://irsa.caltech.edu/applications/DUST

partial exception of HR Del and DN Gem (which may suffer of some local circumstellar reddening), are generally higher than or, at best, equal to the UV and other estimates, where V603 Aql is an extreme case, with a discrepancy of a factor of about 60 (see also Harrison et al. 2013).

Column (15) of Table 8 gives the total galatic extinction derived from the neutral hydrogen maps of the LAB survey (Kalberla et al. 2005)[4]. For this we have assumed an average gas-to-dust ratio $N_{\rm H}/E_{B-V} = 6 \pm 2 \times 10^{21}$ cm^{-2} mag^{-1} (Dickey & Lockman 1990). The E_{B-V} values derived in this way are, on average, in fair agreement with those derived using the Schlegel (1989) maps, but with a rather large scatter.

5. The continuum energy distribution

In IUE spectra, the continuum shortward of 1250 Å is generally affected by the presence of a wide interstellar-circumstellar Ly-α absorption and by a strong geo-coronal Ly-α emission line, while the continuum longward of 3050 Å is typically of low quality because of the strong decrease in camera sensitivity. Therefore, in the present study, these region have been ignored when tracing the continuum.

For each object the continuum was first "hand traced" in the dereddened $\lambda\lambda$ 1250–3050 Å spectrum using line-free regions and then fitted with a powerlaw $F_\lambda \sim A{\cdot}\lambda^{-\alpha}$ distribution using the IRAF stsdas.analysis.fitting.nfit1d application. This code fits one-dimensional nonlinear functions (BB, PL, and combinations thereof) to the data. The nonlinear fitting can be performed by any of two algorithms to minimize the χ^2 fitting: the downhill simplex ("amoeba") or the Levenberg-Marquardt.

The α indexes of the power-law distribution were derived by separate fittings for the SM and the CCM dereddened continua, and for each of the estimated E_{B-V} and their lower and upper limits. We also used a less subjective method to determine the best fitting reddening and power law index at the same time (i.e., by fitting a reddened power law to the observed spectra). We did this using the SM and CCM, as well as the Seaton (1979) $X(\lambda)$ curves. The method was based on a linear fit in logarithm space of the function $K + \alpha\ \log(\lambda) - 0.4\ E(B-V)\ X(\lambda)$ to the log(flux). The continuum was determined automatically by the procedure and by using the local rms distribution to exclude regions with emission lines.

The outputs of the procedure were the parameter values with the corresponding formal uncertainties. The uncertainties are generally smaller than those we derived using the methods described above, while the values are very similar. For this reason we decided to maintain in Table 9 the more conservative estimates for the uncertainties derived in the previous section.

The dereddened UV continuum energy distribution of our old novae is described by a power-law with the spectral index α in the range 0.32–2.55 for the SM extinction law, and 0.35–2.88 for the CCM law (see Table 9, Cols. 3 and 4). The only possible exception is GK Per, which shows a nearly flat continuum that weakens towards the far UV.

Table 9 gives, in separate columns for the CCM and SM reddening curves, the values with the relative uncertainties for all the derived quantities. The E_{B-V} values from Table 8 have been repeated for convenience in Col. 2. Columns 3 and 4 give the index α for the CCM and the SM case, respectively, and Cols. 5 to 8 give (in 10^{-10} erg cm^{-2} s^{-1}) the dereddened UV $\lambda\lambda$ 1200–3200 Å integrated spectral distribution (i.e., the λ-integrated UV fluxes) and the UV $\lambda\lambda$ 1200–3200 Å integrated power-law approximation flux for the CCM and SM cases, respectively.

As expected (see previous section, the index α is systematically higher in spectra dereddened with the CCM law and the difference with the corresponding spectra dereddened with the SM law increases with E_{B-V} from $\Delta\alpha = 0.00$ (RR Pic, $E_{B-V} = 0.00$) to $\Delta\alpha \sim 0.34$ (T Aur and V841 Oph, $E_{B-V} = 0.42$–0.44). Moreover, the range of α values for each object determined using the CCM curve is less than the one determined using the SM curve (see Cols. 3 and 4 in Table 9).

The values of Table 9 also show, as expected, that the relative uncertainty for the integrated flux depends on the uncertainty in E_{B-V}. For an average uncertainty in E_{B-V} of ±0.06 mag, the relative uncertainty in the integrated flux is on the order of 40 %. Therefore, UV luminosities will suffer from the combination of this uncertainty plus that of the distance.

It should be noted that there is neither an indication of nor a requirement for any high-temperature component in the SED: we have tried to "force" such a presence by making a guess for the initial coefficients in a black-body plus power-law fit but the algorithm has indicated a fit with a single power-law, or, alternatively, a fit with a single BB of temperature in the range 1.5×10^4–4.5×10^4 K, but with much higher rms. Therefore, we have chosen the power-law fit that is also supported by physical arguments since it would be difficult to ascribe a single temperature to the most plausible source of the continuum, the accretion disk.

Our UV-based values of the spectral index α are, in any case, systematically lower than those reported for the objects in common by Ringwald et al. (1996) in their optical study. Undoubtedly this comes from the much higher reddening correction they applied to their observed continua.

In the conclusion of this section we observe that the FUSE spectra tend to show a flattening of the SED shortward of λ 1200 Å, where a convincing example is that of the SED of RR Pic (Fig. 2). For this object there is no uncertainty in the reddening correction in the EUV region, since $E_{B-V} = 0.00$. Figures 7 and 8 give the CCM reddening-corrected UV spectra and the corresponding power-law approximation for the 18 old novae in the sample.

6. The UV emission lines

The IUE and STIS spectra of old novae generally show emission lines, the most common one being C IV 1550 Å. Less common or fainter emission lines are those of N V 1240 Å, Si IV 1400 Å, He II 1640 Å, O III] 1666 Å, and N III] 1750 Å. Table 10 gives the observed wavelength, the observed emission intensity, the emission equivalent width (EW), the line FWHM, and the line identification for each emission line. The LW region is almost featureless in most objects.

We note that in the faintest objects ($m_v \geq 15$), which require long exposure times, some emission features may be spurious and produced by cosmic ray hits falling near the strip of the spectrum and that these hits are quite frequent in images of faint objects, taken with long exposure times (above three hours). However, for these objects, the reality of the emission lines listed in Tables 10 and 11 has been confirmed by the detailed inspection of the 2D spectral images (SILO).

It is not easy to associate a definite trend, i.e. a ionization and excitation sequence, to the presence itself and to the relative intensity of the common emission lines (C IV 1550, He II 1640, N V 1240, Si IV 1400) in the various objects. However, it is quite

[4] http://www.astro.uni-bonn.de/hisurvey/profile/index.php

Table 9. Main results for the 18 old novae.

Object	E_{B-V}	α(CCM)	α(SM)	$\int_{UV}^{CCM} PL_\lambda d\lambda$	$\int_{UV}^{CCM} F_\lambda d\lambda$	$\int_{UV}^{SM} PL_\lambda d\lambda$	$\int_{UV}^{SM} F_\lambda d\lambda$	V_{PLr}^{CCM}	V_{PLr}^{SM}	m_V^{obs}
V603 Aql	0.08 ± 0.02	2.07 ± 0.05	2.01 ± 0.04	17.86	$17.43^{+2.64}_{-2.58}$	17.08	$17.20^{+2.60}_{-2.48}$	11.50 ± 0.10	11.45 ± 0.11	11.7 ± 0.1
T Aur	0.42 ± 0.08	2.73 ± 0.25	2.39 ± 0.16	2.51	$2.52^{+2.17}_{-1.16}$	2.38	$2.37^{+1.96}_{-1.07}$	15.45 ± 0.36	15.10 ± 0.46	15.2 ± 0.3
Q Cyg	0.26 ± 0.06	1.20 ± 0.20	1.02 ± 0.15	0.73	$0.73^{+0.40}_{-0.27}$	0.71	$0.71^{+0.39}_{-0.25}$	14.48 ± 0.28	14.31 ± 0.31	14.9 ± 0.6
HR Del	0.17 ± 0.02	2.31 ± 0.05	2.20 ± 0.04	23.86	$23.70^{+4.00}_{-3.33}$	23.25	$23.20^{+3.70}_{-3.30}$	11.72 ± 0.11	11.61 ± 0.12	12.1 ± 0.1
DN Gem	0.17 ± 0.04	1.74 ± 0.09	1.65 ± 0.07	0.52	$0.53^{+0.18}_{-0.14}$	0.52	$0.52^{+0.17}_{-0.14}$	15.18 ± 0.21	15.09 ± 0.24	15.5 ± 0.5
DQ Her	0.05 ± 0.02	0.35 ± 0.06	0.32 ± 0.05	0.22	$0.28^{+0.05}_{-0.04}$	0.22	$0.28^{+0.04}_{-0.04}$	14.18 ± 0.09	14.16 ± 0.10	14.3 ± 0.3
V446 Her	0.38 ± 0.04	2.07 ± 0.12	1.78 ± 0.09	0.22	$0.24^{+0.08}_{-0.06}$	0.23	$0.23^{+0.08}_{-0.06}$	17.17 ± 0.18	16.87 ± 0.22	16.9 ± 0.8
V533 Her	0.03 ± 0.02	1.36 ± 0.05	1.35 ± 0.04	0.70	$0.68^{+0.11}_{-0.09}$	0.68	$0.68^{+0.11}_{-0.10}$	14.02 ± 0.10	14.00 ± 0.11	14.5 ± 0.5
CP Lac	0.28 ± 0.06	1.74 ± 0.14	1.58 ± 0.10	0.64	$0.72^{+0.43}_{-0.26}$	0.62	$0.70^{+0.40}_{-0.25}$	15.30 ± 0.35	15.14 ± 0.38	15.5 ± 0.3
DI Lac	0.26 ± 0.04	2.00 ± 0.10	1.84 ± 0.08	1.69	$1.64^{+0.58}_{-0.44}$	1.58	$1.57^{+0.56}_{-0.40}$	14.54 ± 0.21	14.38 ± 0.24	14.7 ± 0.3
DK Lac	0.22 ± 0.06	2.18 ± 0.14	2.05 ± 0.09	0.24	$0.26^{+0.15}_{-0.10}$	0.23	$0.25^{+0.14}_{-0.09}$	16.72 ± 0.35	16.60 ± 0.38	16.8 ± 0.4
HR Lyr	0.18 ± 0.06	1.15 ± 0.14	1.06 ± 0.10	0.30	$0.30^{+0.17}_{-0.11}$	0.30	$0.30^{+0.16}_{-0.11}$	15.13 ± 0.35	15.04 ± 0.38	15.5 ± 0.3
BT Mon	0.24 ± 0.06	1.33 ± 0.18	1.17 ± 0.14	0.25	$0.29^{+0.17}_{-0.11}$	0.27	$0.28^{+0.16}_{-0.10}$	15.74 ± 0.30	15.56 ± 0.34	15.8 ± 0.6
GI Mon	0.10 ± 0.04	1.43 ± 0.08	1.38 ± 0.06	0.20	$0.19^{+0.06}_{-0.05}$	0.18	$0.18^{+0.07}_{-0.04}$	15.65 ± 0.24	15.60 ± 0.27	15.8 ± 0.8
V841 Oph	0.44 ± 0.06	2.88 ± 0.17	2.55 ± 0.11	13.04	$12.97^{+7.38}_{-4.80}$	12.20	$12.07^{+6.96}_{-4.36}$	13.92 ± 0.30	13.58 ± 0.36	13.5 ± 0.3
GK Per	0.34 ± 0.04	0.12 ± 0.01	0.11 ± 0.01	1.18	$1.19^{+0.65}_{-0.41}$	1.20	$1.17^{+0.39}_{-0.28}$	13.09 ± 0.02	13.09 ± 0.02	13.4 ± 0.4
RR Pic	0.00 ± 0.02	1.67 ± 0.04	1.67 ± 0.03	7.26	$7.24^{+1.19}_{-0.00}$	7.26	$7.23^{+1.12}_{-0.00}$	11.72 ± 0.12	11.72 ± 0.13	12.0 ± 0.2
CP Pup	0.20 ± 0.04	1.59 ± 0.09	1.48 ± 0.07	1.02	$0.98^{+0.34}_{-0.26}$	0.96	$0.96^{+0.32}_{-0.25}$	14.39 ± 0.21	14.27 ± 0.24	15.0 ± 0.5

Notes. From left to right: the color excess E_{B-V}, the index α of the power-law approximation of the CCM (Cardelli et al. 1989a,b) reddening corrected SED, the same for the SM (Savage & Mathis 1979) reddening corrected SED, the λ-integrated UV flux (in 10^{-10} erg cm^{-2} s^{-1}) for the CCM power-law approximation, the CCM dereddened spectral distribution, the SM power-law approximation, and the SM dereddened spectral distribution, respectively. The last three columns give, respectively, the expected observed V-magnitude from the extrapolation of the CCM UV power law after reddening for the visual extinction $A_V = 3.10 \times E_{B-V}$, the same from the extrapolation of the SM UV power law, and, finally, the observed visual magnitude.

surprising that the He II λ 1640 line is very weak or absent in several objects of our sample (i.e. T Aur, Q Cyg, DN Gem, CP Lac, DI Lac, DK Lac, GI Mon, V841 Oph), while the λ 4686 line is generally reported in all old novae (see Kraft 1964; Warner 1976; Williams 1983; Duerbeck & Seitter 1987; Ringwald 1996; Bode & Evans 2008b; Bianchini et al. 2012), with the only possible exception of DK Lac. This contrasts with an expected line ratio λ 1640/λ 4686 close to 7.0 (Dopita & Sutherland 2003). The interpretation of this finding is not straightforward. Neglecting the possibility of a systematic misidentification of the λ 4686 line by several authors in different papers, we tentatively give possible explanations here, which are not mutually exclusive:

1. The observations are not simultaneous.
2. The IUE data have lower spectral resolution and lower S/N.
3. The continuum in the region around λ 1640 Å is stronger by a large factor than around λ 4686 Å, resulting in a reduction of the contrast between the line and the continuum that may mask the λ 1640 Å emission.
4. It is likely that the large optical depth in the He II Ly-α line at λ 304 Å and its complex line transfer in the region where He++ recombines may affect the intensity of the He II Balmer-α line at λ 1640 Å since the lower level of the λ 1640 line is the upper level of the He II Ly-α line. The "trapping" of the He II Ly-α λ 304 line may cause overpopulation of level 2 and, as a consequence, the λ 1640 line develops some optical depth with reabsorption of λ 1640 photons (see also Selvelli et al. 2007). Instead, the level 3 of He II, which is the lower level of the 4686 line, is not affected by overpopulation and reabsorption.

Table 12 lists the stellar emission lines found in FUSE spectra, together with their observed emission intensity, FWHM, and identifications. In the FUSE spectra of CVs, the stellar emission lines are easily distinguished from the spurious emission lines of geo-coronal origin, owing to the fact that the stellar ones have FWHM of a few Å, in contrast with the *FWHM* ~ 0.25–0.35 Å of the latter.

6.1. The uncommon emission features

As already mentioned in Sect. 2.1, for the brightest objects (i.e., V603 Aql, RR Pic, HR Del, DQ Her, and GK Per), we obtained averaged spectra by co-adding all the SW and LW spectra that are well exposed and well centered. The significant improvement in the S/N has led to detecting weak emission features whose reality was otherwise dubious from the inspection of individual spectra. See the IUE spectra of V603 Aql and RR Pic in Figs. 1 and 2.

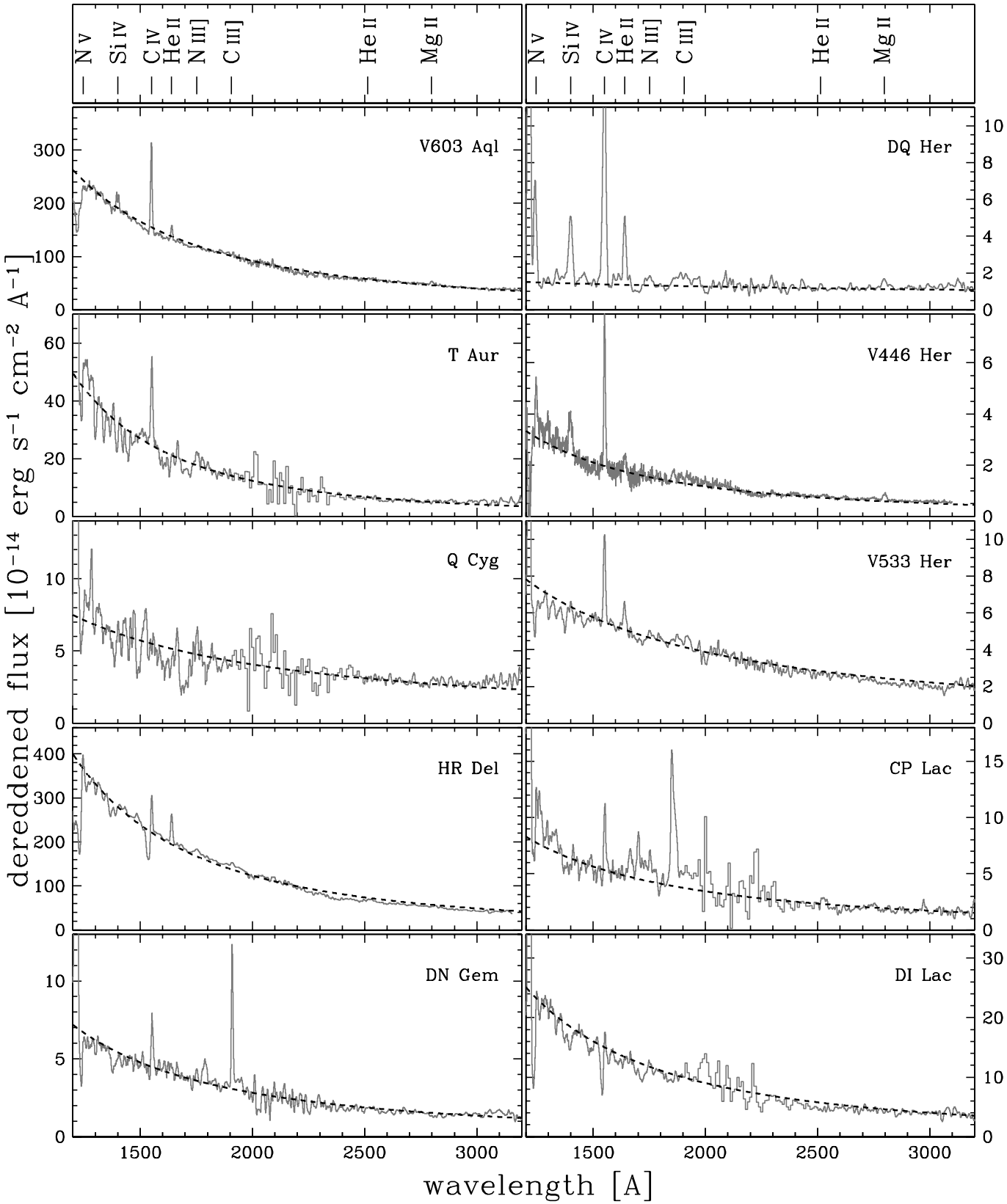

Fig. 7. CCM reddening-corrected IUE spectrum (with the exception of V446 Her: HST-STIS) and the power-law approximation to the continuum SED for ten old novae in the sample. The strong noise generally present between 2000 and 2400 Å is due to the low sensitivity in this range of the IUE LW cameras. For the faintest objects, a modest rebinning has been applied in this wavelength region.

It is of course not surprising that several of these weak features have not been listed in previous UV studies of old novae and CVs, where only the strong and well known lines have generally been included (e.g., N v, Si iv, C iv, He ii). However, it is notable that most of these emission lines are not present in the UV spectra of other classes of emission line objects either

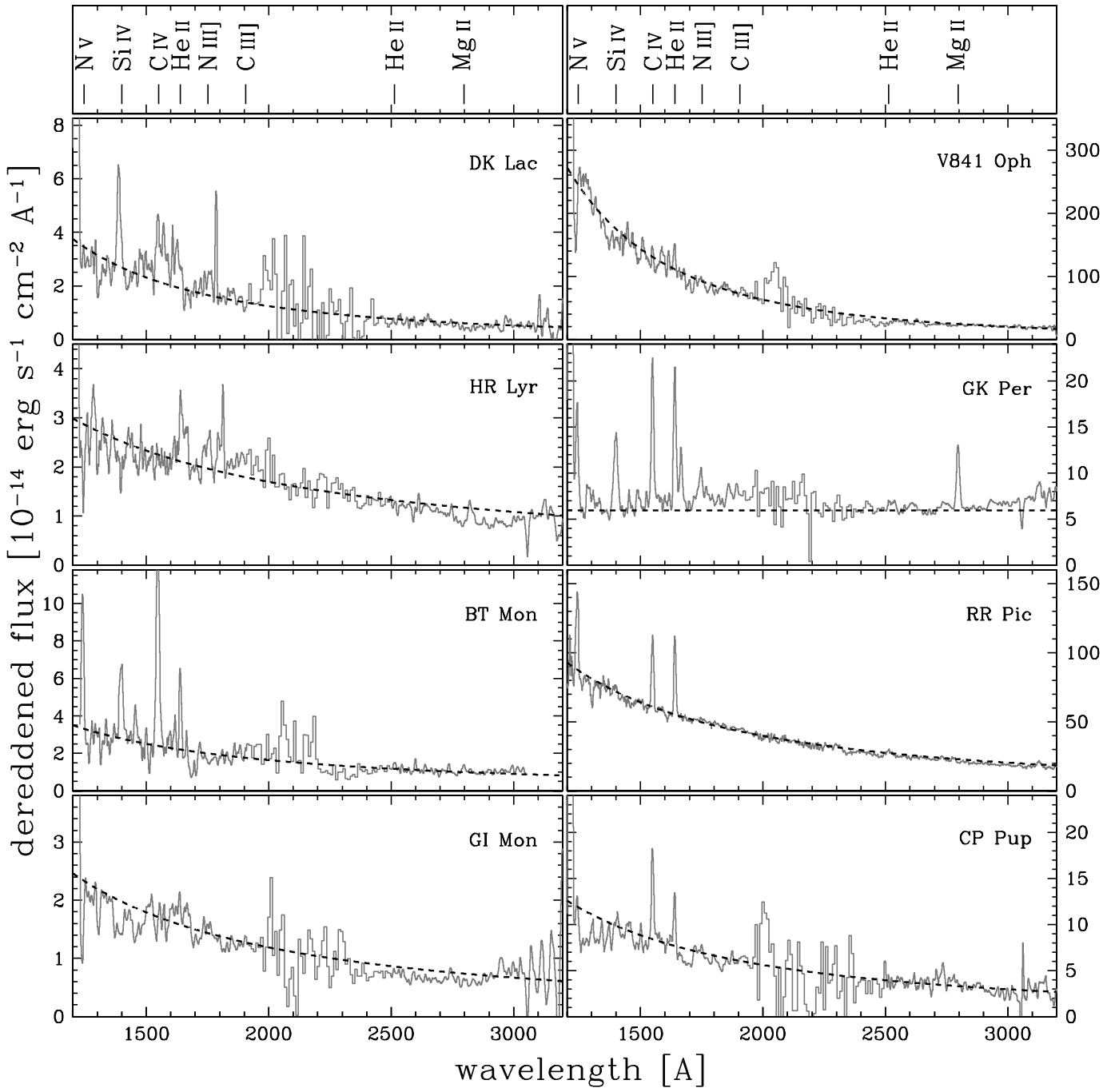

Fig. 8. Same as Fig. 7 for the remaining novae in the sample.

(e.g., other CVs, PNe, symbiotic stars, H II regions). Identifying these lines, see Table 11, is therefore quite difficult or only tentative, in spite of a rather extensive search in the literature and in the lists of atomic lines.

We tentatively suggest that these emission lines may come from regions other than the hot component (accretion disk plus boundary layer), possibly from the irradiated chromosphere of the M dwarf companion, as suggested by the character of some of the proposed identifications. The need to understand the effects of the strong irradiation of the dwarf M stars by the primaries in CVs systems has been explicitely considered by Hilditch (2001).

It should also be noted that the near coincidence in wavelength of several of these weak emission features in different objects gives support to their reality: the line near 1280 Å is present in DQ Her and GK Per, the line near 1434 Å in V603 Aql and HR Del (and also in T Pyx, see Gilmozzi & Selvelli 2007), the line near 1590 Å in V603Aql and RR Pic, the line near 1914 Å in V603 Aql and DQ Her, the line near 3124 Å in V603 Aql, DQ Her, and RR Pic. It is tempting to identify this last feature as the strong O III Bowen line λ 3132 Å, although the wavelength separation is systematically too large.

6.2. The emission features outside the spectrum

As mentioned above and in Sect. 2.1 (IUE), the reality of the emission features present in the extracted spectrum has been carefully checked in the 2D image (SILO), especially for faint

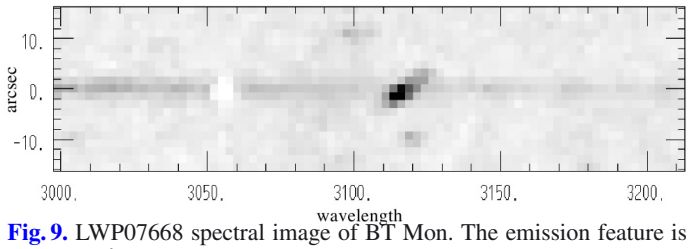

Fig. 9. LWP07668 spectral image of BT Mon. The emission feature is at λ 3116 Å, unidentified.

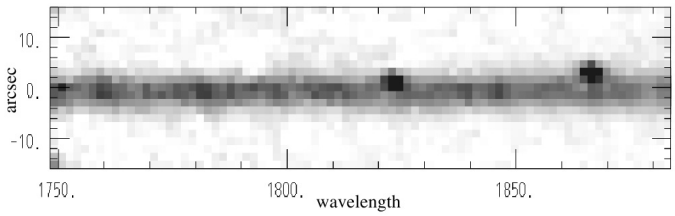

Fig. 10. SWP29325 spectral image of DI Lac with two emission features at λ 1823 Å (S II(2) ?) and at λ 1868 Å(Al III 1863 ?).

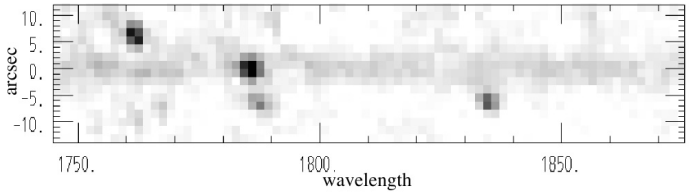

Fig. 11. SWP36701 spectral image of DK Lac with emission features near λ 1761 Å (C II (10) ?), λ 1785 (Fe II (191)), and λ 1835, unid.

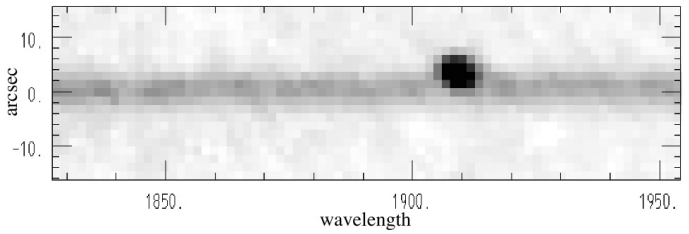

Fig. 12. SWP38213 spectral image of DN Gem with a strong feature near C III] (0.01) λ 1908.

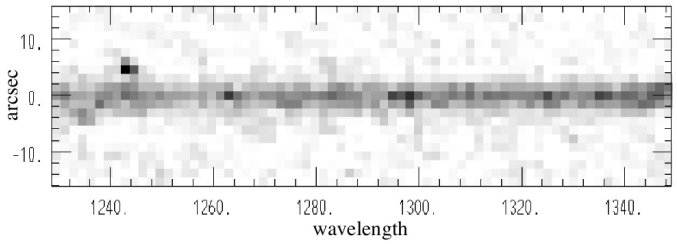

Fig. 13. SWP27806 spectral image of CP Pup, with external features on either side of N V(1) λ 1243.

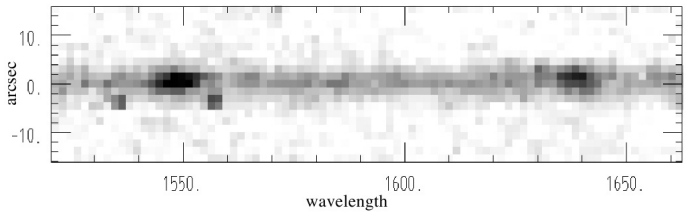

Fig. 14. SWP44789 spectral image of CP Pup with two external features at λ 1535 and λ 1557, likely associated to the λ C IV 1548 line. The other emission line in the spectrum is He II λ 1640.

objects. The detailed examination of these 2D images has led, as an extra result, to detection of several emission features *outside* the central strip of the spectrum but still inside the 20 arcsec large aperture.

We recall that the shape of the large entrance aperture of the IUE SWP spectrograph is that of a rectangle whose projected size on the camera faceplate has approximate dimensions of 10×20 arcsec. The direction of the dispersion is nearly perpendicular to the major axis of the aperture. Therefore, on the SILO images of an extended object (nebula), one expects to see spectral features on both sides of the star spectrum, out to a distance of ± 10 arcsec.

Actually, the IUE large apertures have parallel sides and rounded ends (Bohlin et al. 1980). The full length to the tips of the rounded ends and the width of the SWP's large aperture were measured before flight, and the effective dimensions are 23.0×10.3 arcsec. The IUE NEWSIPS manual, Table 2.1 (Garhart et al. 1997) instead gives a large aperture length of 21.65 ± 0.39 arcsec and a large aperture width of 9.07 ± 0.11 arcsec, but the reported large aperture area (215.33 arcsec^2) is quite a bit larger than the product of the quoted length and width, and it is probable that the length does not include the two rounded ends. The precise form and size of the IUE large aperture is apparently not well-defined (see also González Delgado & Pérez 2000), but can be considered as intermediate between a rectangle and an ellipse.

In the present study we conservatively chose to consider only features at a distance of $\leq$10 arcsec on either side of the central strip for well-centered objects. We note that some pseudo-emission features in the 2D images are produced by the permanent presence of "hot pixels". (For example, a typical one falls near 1750 Å, nearly the same wavelength as a well-known N III] line, though outside the typical position of well-centered spectra.) We also note that emission spikes might be caused by cosmic ray hits mimicking the PSF of IUE. However, there are cases where the spikes either are strictly associated with known emission features present in the (main) spectrum or show a pattern that can hardly be attributed to the impact of cosmic rays.

In general, the external features, if they are not artifacts, should originate in an extended region surrounding the system (nebula, circumstellar envelope, jets). Figures 9 to 14 give some examples of external emission lines found in the IUE spectral images of BT Mon, DI Lac, DK Lac, DN Gem, and CP Pup and should clearly illustrate the problems one encounters in the assessment of the nature and origin of these features. We point out, in any case, that the fact that only one or, at most, a few external features are present in an image (rather than an entire spectrum of several emission lines) is quite difficult to explain.

Downes & Duerbeck (2000) and Bode and Evans (2008c) have provided descriptions of novae with resolved nebular remnants. These include BT Mon, DK Lac, DN Gem, and CP Pup. These objects, with the possible exception of DN Gem, have shell radii smaller than 10 arcsec, i.e. within the width of the IUE large aperture.

7. The absorption lines

In general, the presence of absorption features is limited to the spectral region shortward of λ 1600 Å. We recall that IUE data are affected by camera reseau marks that fall within the spectral region, producing pseudo-absorption features in the extracted

spectrum. These features fall near λ 1320, 1460, 1580, 1720, and 1860 Å and are quite easily recognized by their sharpness.

Most of the true absorption lines in IUE spectra can be identified as the well-known resonance transitions of ionized metals, i.e. Si II 1190 Å, Si II 1260 Å, O I+Si II 1303 Å, C II 1335 Å, and Si IV 1400 Å, C IV 1550 Å, N V 1240 Å, from a higher ionization stage. Unfortunately, the limited resolution of the IUE low-resolution spectra (*FWHM* ~ 5.0 Å) has not allowed estimating the intrinsic line profiles and detecting line components. An interstellar (IS) contribution to the zero-volt component in some of these lines is expected, but the general absence of any absorption near Mg II 2800 Å indicates that it should be minor. This seems confirmed by the lack of definite correlation between the line equivalent widths and parameters, such as the reddening E_{B-V} and the distance (see also Paper II). Also, the rich absorption spectrum of RR Pic, which has a short distance and $E_{B-V} = 0$, clearly suggests that the absorption lines detected in its IUE spectra mainly have a stellar origin, as confirmed by the FUSE spectrum (see the following).

Only two objects, HR Del and DI Lac, show clear wind signatures, such as P Cyg profiles or displaced absorptions. In V603 Aql, these features are weak and only appear in a few spectra.

In FUSE spectra, the much higher spectral resolution allows an immediate separation of the IS components (*FWHM* ~ 0.16–0.24 Å) from the stellar ones (*FWHM* ~ 2.0–4.0 Å). Therefore, for RR Pic, V533 Her, and DI Lac (quite noisy), the stellar absorption lines have been measured and listed in Table 14. DQ Her does not show any IS components, while the FUSE spectrum of V603 Aql shows an extremely rich spectrum of interstellar/circumstellar lines, most of them attributable to the Werner bands of molecular hydrogen. The crowding of these lines has prevented any reliable measurements of the stellar components, whose existence itself has not been clearly established.

The HST-STIS spectrum of DI Lac (see also Moyer et al. 2003) is the only HST-STIS spectrum of an old nova taken at medium-high resolution (R = 45 800, E140M grating), and it allows a clear separation between the IS lines (*FWHM* ~ 0.6–1.5 Å, *EW* ~ 0.2–0.8 Å, mostly once-ionized metals), and the "stellar" ones (*FWHM* ~ 5–12 Å, *EW* ≥ 3.0 Å, higher ionization), as listed in Table 14. We recall that DI Lac has $E_{B-V} = 0.26$ and is at a rather large distance, $d \sim 2000$ pc (Moyer et al. 2003; Puebla et al. 2007) compared to the other old novae. Therefore, the values of the EW of its IS lines (0.2–0.8 Å) can be used as reference for a rough estimate of the IS contribution in the IUE and HST-STIS low resolution spectra.

In the HST-STIS spectra of T Aur and V446 Her taken at low resolution (R ~ 1000, G140L grating), it is not possible to clearly establish the nature of the absorption lines from their profile. However, judging from the equivalent widths, the only absorption feature detected in V446 Her (λ 1260.45 Å, W = 0.61 Å, *FWHM* 2.12 Å) is probably interstellar, while the several absorption lines of T Aur (W ~ 2–5 Å, *FWHM* ~ 4–12 Å) are mainly stellar (see Table 14) and, notably, cover a wide ionization range, from O I to N V.

It is worth noting that for both DI Lac and T Aur there is satisfactory agreement between the EW measurements, for the lines in common, in STIS and IUE spectra, despite the large difference in spectral resolution.

In conclusion, from the examination of the EW and FWHM listed in Tables 13 and 14, one can infer that in IUE spectra the absorption lines of higher ionization e.g N V 1240. Si IV 1400, C IV 1550 have primarily a stellar origin, while those of once ionized metals, such as Si II 1260, Si II (+ O I) 1300, C II 1335, and Si II 1525, may have a non-negligible interstellar or circumstellar contribution. However, this statement needs confirmation from new data at high resolution.

8. The UV SED and the optical magnitudes

The extrapolation of the power-law fits of the UV SED obtained with the CCM and SM reddening laws to λ 5500 Å (the $\lambda_{\rm eff}$ of the V-band for a hot star) yields fluxes that can be converted to visual magnitudes using the zero mag absolute calibration (Gray 1992): $\log F_\lambda = -0.4 \cdot V - 8.45$ (erg cm^{-2} s^{-1} Å^{-1}). To be compared with the observed visual magnitudes, these $V_{\rm PL}$ values have been "reddened" with the visual extinction Av obtained from the E_{B-V} values of Col. 2 in Table 8 assuming $A_V = 3.1\,E_{B-V}$. The results are given in Cols. 9 and 10 of Table 9 for the CCM and the SM cases, respectively, while the observed optical magnitude is given in the last column.

The numbers in Cols. 9 and 10 of Table 9 show that the power-law "reddened" values, $V_{\rm PLr}$, are quite close to those of the observed magnitudes, although slightly brighter, with a cumulative difference of about –3.2 mag if the CCM reddening curve is adopted. The SM curve systematically yields slightly higher luminosities than in the CCM case.

We interpret these results as indicating that the quiescent optical magnitude m_V corresponds to the "tail" of the UV continuum distribution and that the contributions to the V flux by other components (e.g., the WD, the companion star, the hot spot) is of the second order. In other words, the observed V comes mainly from the accretion disk. See, however, the considerations about V603 Aql in the last part of this section.

The main contribution to the observed SED cannot have its origin in a white dwarf. As mentioned in Sect. 5, fitting a BB to the dereddened continua yields temperatures in the range 15 000 to 45 000 K. However, simple calculations based on black body and model white dwarf emissivities[5] and common values for the nova distances indicate that for this range of temperatures, a white dwarf with $M \sim 1.0\,M_\odot$ and $R_1 \sim 5.6 \times 10^8$ cm cannot produce the observed flux at UV and V wavelengths unless a distance smaller by a factor of about 10 is assumed, in blatant contrast to the nova distances in the literature obtained using the common methods of MMRD and expansion parallaxes (see also Moyer et al. 2003). See also the distances derived very recently by Harrison et al. (2013) using the HST Fine Guidance Sensors.

This confirms previous findings (see Hilditch 2011) that have suggested that, with the exclusion of the quiescent phase of a dwarf nova, the white dwarf is generally well hidden in the optical and UV spectrum of the accretion disk. Similar considerations can be used to also exclude the companion star (generally an M2-M5 main-sequence star) as the main contributor to the observed V magnitude. Simple calculations based on the M_v values of M2-M5 V stars and the observed m_v and A_v values would require distances that are lower by at least one order of magnitude than those in the literature.

The literature values of $m_V^{\rm min}$, reported in Col. 11 of Table 9, have been obtained from various sources, such as Duerbeck (1981, 1987); Bruch & Engel (1994); Warner (1995); Downes & Duerbeck (2000); Downes et al. (2001a,b); Bode & Evans (2008a); Collazzi et al. (2009); Ritter & Kolb (2010); and Szkody (1991). We recall that in some objects (V446 Her, BT Mon, V841 Oph, GK Per), $m_V^{\rm min}$ is not univocally established,

[5] See the Rauch models at http://astro.uni-tuebingen.de/~rauch/

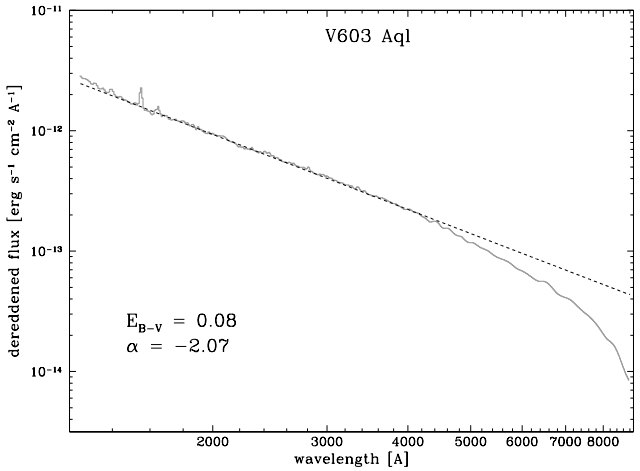

Fig. 15. HST-FOS spectrum of V603 Aql after reddening correction for $E_{B-V} = 0.08$ (Table 9). The spectrum is well fit by a power law with the index determined in the UV up to the B band.

a consequence of intrinsic short-time variations connected with rotational and pulsational phenomena, orbital motions, dwarf-nova-like behavior, etc. (see Bianchini 1990). If various m_V values were available we chose those that were closest to the epochs of the IUE observations.

The FOS spectrum of V603 Aql is a remarkable illustration of a real object whose spectral energy distribution from the far UV to the blue is very close to the one expected in the case of a theoretical accretion disk. In fact, it may help shed some light on why the power law extrapolation to the V band for most of the novae in the sample tends to be brighter than the measured one.

Figure 15 shows a log plot of the spectrum, dereddened using the CCM values of Table 9. (A linear plot would not show the progressive departure from a power law starting at $\lambda \sim 4300$ since it would compress it within a few per cent of the y-axis.) As in the case of T Pyx, which shows a very similar behavior (Gilmozzi & Selvelli 2007), we interpret this departure as an indication that the contribution of the disk to these wavelengths comes from its outer region, where it becomes optically thin (or reaches a physical edge) and is the superposition of the blackbody tails from the progressively larger and cooler last optically thick outer annuli of the disk. The temperature of this outer region of the disk was estimated at ∼10 000 K for T Pyx, and this seems to the case for V603 Aql as well, since the wavelength at which the departure starts is very similar for the two objects.

It is very tempting to ascribe the V magnitude discrepancy between the power law extrapolations and the observed values in Table 9 to a similar effect, i.e., that starting somewhat shortward of the V band, the spectrum of the novae is due to the tail of the emission from the outermost regions of the disk. Wide wavelength coverage spectra similar to that of V603 Aql (or at least a homogeneous set of optical and infrared magnitudes) would be needed to confirm this interpretation and could be used, in principle, to determine the physical size of the disks.

9. Concluding summary

We have analyzed all the available archive UV data for the 18 objects of the sample to determine the spectral characteristics of novae in their quiescent phase, several years after outburst. The main results of this study are:

1. For the 18 old novae in the sample, we have obtained the first set of homogeneous and reliable E_{B-V} values based on the averages of all the best exposed IUE (and STIS) spectra.
2. With the possible exception of GK Per, the dereddened UV continuum is well represented by a single-curve power-law distribution $F_\lambda \propto \lambda^{-\alpha}$, with α in the range 0.3–2.9. We interpret this as a clear indication that the SED comes from an accretion disk.
3. There is good agreement between average spectra taken by different instruments and at different epochs: this indicates a near constancy of the SED over years and a nearly constant mass accretion rate if the SED comes from an accretion disk.
4. The power-law approximation to spectra corrected with the CCM reddening curve yields systematically higher α indexes than those corrected with the SM curve, thanks to its steeper correction below 1500 Å.
5. The extrapolation of the UV power laws to the optical range yields magnitudes that, after having been "reddened" with the new $A_V = 3.1 \times E_{B-V}$ values, are in good agreement with the observed V magnitudes, although slightly brighter. We interpret this as an indication that in the visual region the SED is disk-dominated and that the contributions to the V-band by the WD and/or by the secondary star is only minor. This also confirms that accretion is through a disk that accounts for most of the UV-optical energy distribution.
6. The high S/N of the averaged spectra of the brightest objects (e.g., V603 Aql, RR Pic, HR Del) has led to detection of several "new" emission lines, generally not listed in previous studies of CVs and other emission-line objects. However, identifying these features is quite challenging on low-resolution data.
7. A detailed examination of the spectral images has revealed the presence of several emission features outside the main spectrum. Their nature and origin are not clear; it is likely that they originate in circumstellar or nebular material surrounding the system, but further studies are required to confirm this.
8. In IUE spectra, the absorption lines of once ionized metals have a non-negligible IS or CS contribution, while those of higher ionization have primarily a stellar origin.

In Paper II we will combine these results with data on the outburst phases to derive physical parameters and statistical properties of novae in the quiescent and outburst phases.

Acknowledgements. We gratefully acknowledge the participation of Angelo Cassatella to the first stages of this study. We thank John Danziger for reading the manuscript and for valuable comments. The comments and suggestions by the anonymous referee helped in improving the content of the paper considerably.

References

Aidelman, Y., Cidale, L. S., Zorec, J., & Arias, M. L. 2012, A&A, 544, A64
Araujo-Betancor, S., Gänsicke, B. T., Long, K. S., et al. 2005, ApJ, 622, 589
Bianchini, A. 1990, in Physics of Classical Novae, IAU Colloq., 122, 13
Bianchini, A., & Sabadin, F. 1983, A&A, 125, 112
Bianchini, A., Saygac, T., Orio, M., Della Valle, M., & Williams, R. 2012, A&A, 539, A94
Bode, M. F., & Evans, A. 2008a, Classical Novae, 2nd edn. (Cambridge: Cambridge University Press), Cambridge Astrophysics Series, 43, 26
Bode, M. F., & Evans, A. 2008b, Classical Novae, 2nd edn. (Cambridge: Cambridge University Press), Cambridge Astrophysics Series, 43, 29
Bode, M. F., & Evans, A. 2008c, Classical Novae, 2nd edn. (Cambridge: Cambridge University Press), Cambridge Astrophysics Series, 43, 285
Boggess, A., Carr, F. A., Evans, D. C., et al. 1978, Nature, 275, 372
Bohlin, R. C., Sparks, W. M., Holm, A. V., Savage, B. D., & Snijders, M. A. J. 1980, A&A, 85, 1
Borczyk, W., Schwarzenberg-Czerny, A., & Szkody, P. 2003, A&A, 405, 663
Bruch, A., & Engel, A. 1994, A&AS, 104, 79
Cardelli, J. A., Clayton, G. C., & Mathis, J. S. 1989a, ApJ, 345, 245 (CCM)

Cardelli, J. A., Clayton, G. C., & Mathis, J. S. 1989b, Interstellar Dust, 135, 5 (CCM)
Collazzi, A. C., Schaefer, B. E., Xiao, L., et al. 2009, AJ, 138, 1846
Diaz, M. P., & Bruch, A. 1997, A&A, 322, 807
Dickey, J. M., & Lockman, F. J. 1990, ARA&A, 28, 215
Dopita, M. A., & Sutherland, R. S. 2003, Astrophysics of the diffuse universe (Berlin, New York: Springer)
Downes, R. A., & Duerbeck, H. W. 2000, AJ, 120, 2007
Downes, R. A., Duerbeck, H. W., & Delahodde, C. E. 2001a, J. Astron. Data, 7, 6
Downes, R. A., Webbink, R. F., Shara, M. M., et al. 2001b, PASP, 113, 764
Duerbeck, H. W. 1981, PASP, 93, 165
Duerbeck, H. W. 1987, Journal of the British Astronomical Association, 98, 48
Duerbeck, H. W. 1992, MNRAS, 258, 629
Duerbeck, H. W., & Seitter, W. C. 1987, Ap&SS, 131, 467
Engle, S. G., & Sion, E. M. 2005, PASP, 117, 1230
Fitzpatrick, E. L. 1999, PASP, 111, 63
Fitzpatrick, E. L., & Massa, D. 2007, ApJ, 663, 320
Frank, J., King, A., & Raine, D. J. 2002, Accretion Power in Astrophysics, 3nd edn. (Cambridge: Cambridge University Press), 398
Friedjung, M., Puget, P., & Andrillat, Y. 1982, A&A, 114, 351
Friedjung, M., Selvelli, P., & Cassatella, A. 1997, A&A, 318, 204
Froning, C. S., Long, K. S., Gänsicke, B., & Szkody, P. 2012, ApJS, 199, 7
Gänsicke, B. T., de Martino, D., Marsh, T. R., et al. 2006, Ap&SS, 306, 177
Garhart, M. P., Smith, M. A., Turnrose, B. E., Levay, K. L., & Thompson, R. W. 1997, NASA IUE Newsletter, 57, 1
Gilmozzi, R., & Selvelli, P. 2007, A&A, 461, 593
Gilmozzi, R., Selvelli, P. L., & Cassatella, A. 1994, Mem. Soc. Astron. It., 65, 199
González Delgado, R. M., & Pérez, E. 2000, MNRAS, 317, 64
González-Riestra, R., Cassatella, A., Wamsteker W., 2001, A&A 373,730
Gray, D. F. 1992, Camb. Astrophys. Ser., 20
Hamilton, R. T., Urban, J. A., Sion, E. M., et al. 2007, ApJ, 667, 1139
Harrison, T. E., Bornak, J., McArthur, B. E., & Benedict, G. F. 2013, ApJ, 767, 7
Hilditch, R. W. 2001, An introduction to close binary stars (Cambridge: Cambridge University Press)
Kalberla, P. M. W., Burton, W. B., Hartmann, D., et al. 2005, A&A, 440, 775
Kolobow, C., & Sion, E. 2011, PASP, 123, 892
Kovetz, A., Prialnik, D., & Shara, M. M. 1987, Ap&SS, 131, 419
Kraft, R. P. 1964, ApJ, 139, 457
Krautter, J., Vogt, N., Klare, G., et al. 1981, A&A, 102, 337
La Dous, C. 1991, A&A, 252, 100
Livio, M. 1988, 108th IAU Colloq: Atmospheric Diagnostics of Stellar Evolution, 305, 225
Long, K. S. 2006, Adv. Space Res., 38, 2827
Massa, D., Savage, B. D., & Fitzpatrick, E. L. 1983, ApJ, 266, 662
Mauche, C. W., Lee, Y. P., & Kallman, T. R. 1997, ApJ, 477, 832
McElroy, D., Walsh, C., Markwick, A. J., et al. 2013, A&A, 550, A36
Moyer, E., Sion, E. M., Szkody, P., et al. 2003, AJ, 125, 288
Orio, M., Mukai, K., Bianchini, A., de Martino, D., & Howell, S. 2009, ApJ, 690, 1753
Orosz, J. A., & Wade, R. A. 2003, ApJ, 593, 1032
Pottasch, S. R., & Bernard-Salas, J. 2013, A&A, 550, A35
Prinja, R. K., Knigge, C., Ringwald, F. A., & Wade, R. A. 2000, MNRAS, 318, 368
Puebla, R. E., Diaz, M. P., & Hubeny, I. 2007, AJ, 134, 1923
Puebla, R. E., Diaz, M. P., Hillier, D. J., & Hubeny, I. 2011, ApJ, 736, 17
Ringwald, F. A., Naylor, T., & Mukai, K. 1996, MNRAS, 281, 192
Ritter, H., & Kolb, U. 2010, VizieR Online Data Catalogue, B/cb
Rodriguez-Pascual, P. M., González-Riestra, R., Schartel, N., & Wamsteker, W. 1999, A&A, 139, 183
Rosino, L., Bianchini, A., & Rafanelli, P. 1982, A&A, 108, 243
Sankrit, R., & Andersson, B.-G. 2005, in FUSE Data Analysis Cookbook, `fuse.pha.jhu.edu/analysis/cookbook`
Sasseen, T. P., Hurwitz, M., Dixon, W. V., & Airieau, S. 2002, ApJ, 566, 267
Savage, B. D., & Mathis, J. S. 1979, Ann. Rev. Astron. Astrophys. 17, 73 (SM)
Schlegel, D. J., Finkbeiner, D. P., & Davis, M. 1998, ApJ, 500, 525
Selvelli, P. 2004, Baltic Astronomy, 13, 93
Selvelli, P., & Friedjung, M. 2003, A&A, 401, 297
Selvelli, P., Gilmozzi, R., Friedjung, M., & Cassatella, A. 1998, Proc. Ultraviolet Astrophysics Beyond the IUE Final Archive, ESA SP, 413, 435
Selvelli, P., Danziger, J., & Bonifacio, P. 2007, A&A, 464, 715
Seaton, M. J. 1979, MNRAS, 187, 73P
Shafter, A. W. 1997, ApJ, 487, 226
Shara, M. M., Livio, M., Moffat, A. F. J., & Orio, M. 1986, ApJ, 311, 163
Shara, M. M., Zurek, D., De Marco, O., et al. 2012, AJ, 143, 143
Silber, A. D., Anderson, S. F., Margon, B., & Downes, R. A. 1996a, AJ, 112, 1174
Silber, A. D., Anderson, S. F., Margon, B., & Downes, R. A. 1996b, ApJ, 462, 428
Sion, E. M., Gänsicke, B. T., Long, K. S., et al. 2008, ApJ, 681, 543
Szkody, P., Stablein, C., Mattei, J. A., & Waagen, E. O. 1991, ApJS, 76, 359
Verbunt, F., & Wade, R. A. 1984, A&AS, 57, 193
Wade, R. A., & Hubeny, I. 1998, ApJ, 509, 350
Warner, B. 1976, Proc. IAU Symp., 73, 85
Warner, B. 1987, MNRAS, 227, 23
Warner, B. 1995, Camb. Astrophys. Ser., 28
Weight, A., Evans, A., Naylor, T., Wood, J. H., & Bode, M. F. 1994, MNRAS, 266, 761
Williams, G. 1983, ApJS, 53, 523
Wu, C.-C., Holm, A. V., Panek, R. J., et al. 1989, ApJ, 339, 443

Pages 15 to 20 are available in the electronic edition of the journal at http://www.aanda.org

Table 2. Excerpt from the complete list of IUE observations of bright old novae.

Object	Camera	Image	Obs. date	Exp.(s)
V603 Aql	LWR	04994	1979-07-10	359.503
	...	...	...	...
	LWP	32289	1996-05-07	599.531
	SWP	05678	1979-06-29	779.748
	...	...	...	...
	SWP	47794	1993-06-03	899.761
GK Per	LWR	05685	1979-09-24	2699.548
	...	...	...	...
	LWP	11965	1987-10-27	5219.819
	SWP	06623	1979-09-24	10799.793
	...	...	...	...
	SWP	32174	1987-10-27	17999.740
HR Del	LWR	04993	1979-07-10	599.528
	...	...	...	...
	LWP	13136	1988-04-29	719.514
	SWP	02122	1978-07-27	1199.588
	...	...	...	...
	SWP	45482	1992-08-31	1319.601
DQ Her	LWR	07500	1980-04-14	10799.797
	...	...	...	...
	LWP	05512	1985-03-13	1199.595
	SWP	06358	1979-09-02	5399.627
	...	...	...	...
	SWP	25440	1985-03-13	1439.614
RR Pic	LWR	05009	1979-07-11	1799.656
	...	...	...	.....
	LWP	15758	1989-06-19	899.768
	SWP	05774	1979-07-11	599.524
		...	...	...
	SWP	57075	1996-05-08	1079.576

Notes. Complete list of the about 230 spectra used in this paper available in electronic form at the CDS.

Table 3. Observations with IUE: faint old novae.

Object	Camera	Image	Obs. date	Exp.(s)
T Aur	LWP	22601	1992-03-15	10799.800
	SWP	44179	1992-03-15	11 999.512
	SWP	49922	1994-01-31	17 999.740
Q Cyg	LWP	14754	1989-01-02	7199.826
	SWP	35239	1989-01-02	14 159.742
DN Gem	LWP	17402	1990-02-21	19 799.531
	SWP	38213	1990-02-19	17 999.740
V533 Her	LWR	08915	1980-09-30	4499.740
	LWP	23205	1992-05-29	6899.589
	SWP	10250	1980-09-29	13 499.467
	SWP	44805	1992-05-29	17 999.740
CP Lac	LWP	20744	1991-07-04	7799.480
	SWP	42000	1991-07-04	16 019.735
DI Lac	LWP	09208	1986-09-28	7199.826
	SWP	29325	1986-09-28	16 799.613
	SWP	48286	1993-08-02	20 394.752
DK Lac	LWP	15956	1989-07-19	5279.621
	SWP	36701	1989-07-18	17 999.740
HR Lyr	LWP	18163	1990-06-21	20 039.557
	SWP	39145	1990-06-24	24 059.773
BT Mon	LWP	07668	1986-02-16	21 359.697
	SWP	27732	1985-02-17	22 439.805
GI Mon	LWP	17709	1990-04-08	23 399.506
	SWP	38419	1990-03-23	20 399.588
V841 Oph	LWR	06925	1980-02-14	5699.868
	LWP	30470	1995-04-17	2699.551
	SWP	07950	1980-02-14	7199.819
	SWP	54454	1995-04-17	3599.844
CP Pup	LWP	07728	1986-02-27	5099.807
	SWP	27806	1986-02-27	17 999.740

Table 4. Observations with HST-FOS.

Object	Dataset	Date	Exp.(s)	Ap.	Grating
V603 Aql					
	Y2GN0204T	1994-10-12	2085	4.3	G160L
	Y2GN0205T	1994-10-12	1941	4.3	G160L
	Y2GN0206T	1994-10-12	1618	4.3	PRISM
DQ Her					
	Y1DZ0501T	1993-10-15	2169	1.0	G160L
	Y1DZ0601T	1993-10-15	2169	1.0	G160L
	Y1DZ0602T	1993-10-15	2169	1.0	G160L
	Y1DZ0603T	1993-10-15	2400	1.0	G190H
	Y2LU0301T	1995-05-09	1737	1.0	G160L
	Y2LU0302T	1995-05-09	1737	1.0	G160L
	Y2LU0303T	1995-05-09	1737	1.0	G160L
	Y2LU0304T	1995-05-09	2400	1.0	G130H
	Y2LU0601T	1995-04-27	1737	1.0	G160L
	Y2LU0602T	1995-04-27	1737	1.0	G160L
	Y2LU0603T	1995-04-27	1737	1.0	G160L
	Y2LU0604T	1995-04-27	2400	1.0	G190H
	Y2XPA101T	1995-10-13	1717	1.0	G130H
	Y2XPA102T	1995-10-13	2418	1.0	G130H
	Y2XPA103T	1995-10-13	2418	1.0	G130H
	Y2XPA104T	1995-10-13	2243	1.0	G130H
	Y2XPA201T	1995-10-17	1732	1.0	G190H
	Y2XPA202T	1995-10-17	2423	1.0	G190H
	Y2XPA203T	1995-10-17	2418	1.0	G190H
	Y2XPA204T	1995-10-17	1902	1.0	G190H
	Y2XPB201T	1995-10-17	2340	1.0	G130H
	Y2XPB202T	1995-10-17	2418	1.0	G130H
	Y2XPB203T	1995-10-17	2418	1.0	G130H
	Y2XPB204T	1995-10-17	2262.	1.0	G130H

Table 5. Observations with HST-GHRS.

Object	Dataset	Date	Exp.(s)	Apert.	Grating
V603 Aql	Z28K0106T	1994-02-20	2611	0.25	G160M
	Z28K0107T	1994-02-20	2502	0.25	G160M
	Z28K0109T	1994-02-20	1849	0.25	G160M
	Z37V0204T	1996-10-06	1087	2.0	G140L
	Z37V0205T	1996-10-06	544	2.0	G140L
	Z37V0206T	1996-10-06	1305	2.0	G140L
	Z37V0207T	1996-10-06	652	2.0	G140L
	Z37V0208T	1996-10-06	1305	2.0	G140L
	Z37V020AT	1996-10-06	652	2. 0	G140L
	Z37V020BT	1996-10-06	1523	2.0	G140L
	Z37V020CT	1996-10-06	652	2.0	G140L

Table 6. Observations with HST-STIS.

Object	Dataset	Date	Exp.(s)	Apert.	Grating
T Aur	O6LI0M010	2003-03-07	600	52×0.2	G140L
DI Lac	O5B607010	2000-04-19	2127	0.2×0.2	E140M
V446 Her	O8N001010	2003-08-11	2260	52×0.2	G140L
	O8N001020	2003-08-11	2878	52×0.2	G140L
	O8N001030	2003-08-11	2878	52×0.2	G230L
	O8N001040	2003-08-11	2878	52×0.2	G230L

Table 7. Observations of old novae with FUSE.

Object	Dataset	No.	Date	Exp.(s)	Range (Å)
V603 Aql	Q1130101000	8	2002-06-07	16807	980-1181
DQ Her	D9130501000	3	2003-06-30	7816	905-1187
V533 Her	D9131701000	4	2003-07-01	4121	916-1188
DI Lac	D9131301000	3	2003-10-20	6030	905-1187
RR Pic	D9131601000	5	2003-10-29	13564	916-1187
	S7011201000	6	2005-04-05	13298	916-1187
	S7011202000	8	2005-04-05	1926	noisy
	S7011203000	5	2005-04-05	6058	916-1187
	U1071201000	5	2006-01-25	14449	916-1187

Table 10. Wavelengths (Å), observed intensities (erg cm^{-2} s^{-1} Å^{-1}), emission equivalent widths (Å), FWHMs (Å), and identifications for the emission lines. All measurements are from IUE spectra, except T Aur, V446 Her and DI Lac (STIS).

λ_{obs}	Em. int.	*EW*	*FWHM*	Identification
V603 Aql				
1175.2	1.16E-12	–1.05	6.40	C III(4) 1175.70
1394.9	1.30E-12	–1.35	6.68	Si IV(1) 1393.75
1403.1	1.38E-12	–1.43	8.24	Si IV(1) 1402.77
1549.9	8.60E-12	–10.83	8.64	C IV(1) 1548.18+1550.78
1640.6	1.41E-12	–1.94	8.08	He II(12) 1640.47
1666.5	2.33E-13	–0.33	5.96	O III(0.01) 1660.80+1666.15
1760.2	5.74E-13	–0.89	15.29	6x N III 1750
1857.6	4.99E-13	–0.85	15.23	Al III(1) 1854.72
1891.4	4.79E-13	–0.85	17.42	Si III(1) 1892
2302.6	7.70E-13	–2.29	17.24	C III(8) 2296.78
2799.5	6.78E-13	–2.23	15.42	Mg II(1) 2800
T Aur				
1552.2	8.13E-14	–9.18	6.73	C IV(1) 1548.18+1550.78
1641.8	2.57E-14	–3.32	4.24	He II(12) 1640.47
HR Del				
1245.4	1.66E-12	–2.65	7.09	N V(1) 1238.82+1242.80
1484.3	4.50E-13	–0.65	10.26	N IVx2 1487
1551.1	2.32E-12	–3.69	5.23	C IV(1) 1550, P Cyg
1640.1	1.99E-12	–3.41	6.75	He II(12) 1640.47
1751.7	7.13E-13	–1.41	19.45	6x N III 1750
1909.8	2.95E-13	–0.75	9.67	C III] 1906.67+1908.73
DN Gem				
1553.6	1.02E-13	–8.51	9.72	C IV(1) 1548.18+1550.78
1909.6	2.07E-13	–22.04	7.81	C III] 1906.67+1908.73 knot
DQ Her				
1175.9	8.49E-14	–8.72	9.00	C III(4) 1175.70
1241.6	5.06E-13	–50.24	13.95	N V(1) 1238.82+1242.80
1337.7	9.43E-14	–10.46	16.79	C II(1) 1335
1399.3	4.75E-13	–44.98	18.91	Si IV(1) 1393.75+1402.77
1549.9	1.58E-12	–149.90	15.10	C IV(1) 1548.18+1550.78
1640.7	3.68E-13	–36.06	13.51	He II(12) 1640.47
1749.9	9.44E-14	–9.76	33.10	6xN III 1750
1890.1	4.11E-14	–3.72	13.19	S III(1) 1891.66
2796.6	9.57E-14	–10.79	22.85	Mg II(1) 2795.52+2802.70
V446 Her				
1176.4	6.37E-15	–7.28	10.64	C III(4) 1175.70
1246.7	5.63E-15	–6.57	10.53	N V(1) 1238.82+1242.80 ?
1297.9	1.46E-15	–1.45	4.01	Si III 1298.9(?)
1307.0	7.93E-16	–0.77	3.07	Si III 1304.3(?)
1338.4	1.19E-15	–1.07	5.43	C II (1 1335.3+O IV1338 ?
1398.9	1.14E-14	–9.70	17.8	Si IV(1) 1393.75+1402.77
1551.0	3.07E-14	–28.82	8.17	C IV(1 1548.18+1550.78
1640.8	8.62E-15	–8.45	17.68	He II(12) 1640.47
2799.6	5.82E-15	–7.23	18.28	Mg II(1) 2795.52+2802.70
V533 Her				
1550.8	4.71E-13	–10.91	11.21	C IV(1 1548.18+1550.78
1639.7	1.56E-13	–3.78	12.65	He II(12) 1640.47
1666.9	2.14E-14	–0.55	5.76	O III(0.01 1660.80+1666.15
CP Lac				
1552.3	7.48E-14	–11.36	9.58	C IV(1 1548.18+1550.78
1854.9	2.80E-13	–43.85	22.48	Al III(1 1854.72+1862.79 knot?
DI Lac				
1550.8	5.76E-14	–2.49	4.57	C IV(1)1550, P Cyg
DKLac				
1388.4	1.16E-13	–29.02	17.17	knot, Si IV(1)1393.75 ?
1548.7	8.76E-14	–19.77	19.33	C IV(1 1548.18+1550.78
HR Lyr				
1642.2	6.13E-14	–10.66	15.99	He II(12) 1640.47
1661.1	4.77E-14	–8.33	24.84	O III(0.01 1660.80+1666.15
1812.6	4.29E-14	–8.03	8.56	Si II(1)x3 1815+Ne III1815
BT Mon				
1240.2	8.17E-14	–40.03	11.67	N V(1) 1238.82+1242.80
1398.0	1.02E-13	–33.48	18.32	O IV(0.01 1401.40
1547.2	2.51E-13	–76.54	14.73	C IV(1 1548.18+1550.78
1638.9	6.92E-14	–21.4	9.38	He II(12) 1640.47
1664.7	1.48E-14	–5.35	6.29	O III(0.01 1660.80+1666.15
V841 Oph				
1638.8	1.75E-13	–3.91	9.18	He II(12) 1640.47
GK Per				
1241.0	4.68E-14	–16.69	11.60	N V(1) 1238.82+1242.80
1399.5	1.07E-13	–29.06	18.91	Si IV(1) 1393.75+1402.77
1489.8	2.90E-14	–6.66	17.36	N IV (1) 1482.96+1486.23
1524.4	1.22E-14	–2.58	7.40	Si II 1526.70
1549.1	1.52E-13	–29.20	11.55	C IV(1)1548.18+1550.78
1640.3	1.49E-13	–24.51	11.36	He II(12) 1640.47
1665.4	5.18E-14	–8.28	10.27	O III(0.01 1660.80+1666.15
1745.7	4.79E-14	–7.70	17.29	6xN III 1750
1860.4	2.29E-14	–4.05	16.25	Al III(1)x2 1860
1892.8	1.65E-14	–3.00	12.69	Si III] 1892.03
2796.4	1.68E-13	–17.80	14.79	Mg II(1) 2795.52+2802.70
RR Pic				
1220.1	8.30E-13	–1.04	4.51	O V 1218
1241.6	8.07E-12	–10.07	11.72	N V(1) 1238.82+1242.80
1368.7	3.78E-13	–0.51	5.25	O V 1371.30
1395.4	1.08E-12	–1.52	21.91	Si IV(1) 1393.75+1402.77
1549.5	5.76E-12	–9.75	10.29	C IV(1)1548.18+1550.78
1572.1	5.72E-13	–0.99	18.07	Ne V 1575
1640.5	5.59E-12	–10.13	9.06	He II(12) 1640.47
1665.3	1.16E-13	–0.22	3.79	O III(0.01 1660.80+1666.15
2304.9	1.31E-12	–4.45	31.72	Ciii (6) 2296.87+HeII
2515.0	1.07E-12	–4.18	29.95	He II(1) 2511.21
2731.1	3.39E-13	–1.50	12.21	He II(1) 2733.32
3127.1	8.81E-13	–5.17	19.27	O III (12) 3132.79, Bowen?
3201.0	8.34E-13	–5.54	25.17	He II(1) 3203.10
CP Pup				
1240.8	8.32E-14	–6.51	13.27	N V(1) 1238.82+1242.80
1304.4	3.72E-14	–2.64	10.52	Si IIIx2 1299+O Ix4 1304
1371.4	3.16E-14	–2.01	8.24	O V 1371.30
1404.1	7.33E-14	–4.13	17.77	O IV]x2 1402+S IV]x4 1412
1549.1	2.34E-13	–12.04	9.94	C IV(1)1548.18+1550.78
1639.3	1.44E-13	–8.24	9.57	He II(12) 1640.47

Table 11. Observed wavelengths (Å), observed intensities (erg cm^{-2} s^{-1} Å^{-1}), FWHMs (Å), and tentative identifications for the uncommon emission lines in IUE spectra.

λ_{obs}	Em. int.	*FWHM*	Identification
V603 Aql			
1292.5	1.93E-13	4.24	?
1324.5	1.86E-13	9.25	S I(8)x3 1323
1436.5	6.26E-13	12.50	?S I(5)x3 1433
1474.9	4.69E-13	16.84	S I(4)x3 + S I(3)x6 1478
1586.2	1.23E-13	3.31	?
1591.1	2.08E-13	5.51	?
1916.2	3.29E-13	8.42	S I 1914, Fe III(34) 1915
3121.5	2.78E-13	13.48	?
T Aur			
1380.6	1.93E-14	7.71	? SWP49922 only
HR Del			
1316.0	2.42E-13	13.49	Mg V 1317, Si III 1312.59
1350.5	1.32E-13	5.17	Si II(7)x6 1349
1432.33	2.82E-13	11.12	S I(5)x3 1434
DQ Her			
1280.4	1.54E-14	6.96	N IV 1284 + C I(5,6,7,8) 1280
1458.5	8.72E-14	16.73	C I(36,37,38)x3 1564
?			
1613.8	3.62E-14	11.16	Al II] 1611.81
1912.9	2.66E-14	9.81	Fe III(34)? S I 1914
2431.5	3.44E-14	12.26	Ne IV 2425
2646.5	2.47E-14	9.68	?
3125.8	5.57E-14	16.34	?
DK Lac			
1570.8	3.03E-14	9.69	?
1607.8	1.51E-14	5.04	Fe II(8) 1609 ?
1785.4	5.13E-14	6.36	knot ?, Fe II(191) 1788
HR Lyr			
1284.9	2.92E-14	13.41	C I(5) 1280
1812.8	3.28E-14	7.26	?
GK Per			
1282.9	5.26E-15	5.72	C I(5) 1280
1290.7	7.48E-15	10.55	?
1453.6	1.07E-14	6.82	?
1524.4	1.12E-14	6.85	
1860.1	2.00E-14	14.43	
RR Pic			
1168.4	1.35E-12	9.99	C IV(11.19) 1168.90
1211.7	1.34E-12	4.06	?
1507.4	3.46E-13	7.20	O V 1506.88 ?
1575.6	3.01E-13	7.83	?
1588.8	2.31E-13	7.21	?
1681.7	9.82E-14	3.80	?
2834.5	1.39E-13	4.96	?
3127.1	8.41E-13	18.49	O III 3132.9 Bowen ?

Table 12. Observed wavelengths (Å), observed emission intensities (erg cm^{-2} s^{-1} Å^{-1}), equivalent widths W (Å), FWHMs (Å), and identifications for the stellar emission lines in FUSE spectra.

λ_{obs}	Em. int.	*W*	*FWHM*	Identification
V603 Aql				
1175.61	9.83E-13	–0.93	2.50	C III 1175
DQ Her				
1027.29	2.01E-13	–64.52	1.43	Lyβ 1025.67
1031.83	1.32E-13	–9.69	2.16	O VI 1031.9
1037.52	2.49E-13	–30.20	3.11	O VI 1037.6
1062.99	8.82E-14	–18.63	5.57	S IV 1062.66
1072.84	9.43E-14	–18.72	3.35	S IV 1072.97
1085.43	2.01E-13	–36.62	3.17	He II 1084.91 + N II 1085.1
1111.35	8.23E-14	–24.71	6.48	2xSi III 1111.6
1118.13	9.35E-14	–28.40	7.30	P V 1117.98
1127.95	5.91E-14	–9.72	4.64	P V 1128.0 + Si IV 1128.3
1134.70	4.21E-14	–14.94	2.62	N I 1134.3 ?
1175.72	1.97E-13	–85.62	5.45	6*C III 1175
DI Lac				
1042.26	2.36E-14	–9.34	3.06	O I 1041.69 ?
1046.21	2.98E-14	–13.46	2.83	?
RR Pic				
1029.85	2.45E-12	–2.76	4.94	Lyβ 1215.67 +?
1035.11	3.93E-12	–3.15	2.51	O VI 1031.95 + 1037.63
1039.48	2.36E-12	–2.72	4.62	?
1084.60	2.43E-12	–2.76	5.66	N II 83.99 ?

Table 13. Wavelengths (Å), equivalent widths (Å), FWHM (Å), and identifications for the absorption lines in IUE spectra.

λ_{obs}	*EW*	*FWHM*	Identification	λ_{obs}	*EW*	*FWHM*	Identification
V603 Aql				DI Lac			
1262.15	0.52	9.03	Si II(4) 60.42 + Fe II (9) 60.54+	1234.2	10.76	15.36	N V(1) 1238.82 + 1242.80
			S II(1) 59.52	1261.3	2.15	11.44	Si II(4) 60.42 + S II(1) 59.52
1303.9	0.40	4.73	O I(2) 02.17 + Si II(3) 04.37	1301.8	0.73	7.20	O I(2) 02.17 + Si II(3) 04.37
1372.4	0.36	3.93	N III(8) 1370.13 ?	1334.7	1.53	7.89	C II(1) 35.10
				1395.6	3.60	16.70	Si IV(1) 1393.75 + 1402.77
T Aur				1539.4	7.28	13.10	C IV(1) x2 1550, PCyg
1239.8	4.93	10.43	N V(1) 1238.82 + 1242.80				
1299.6	4.79	10.05	S I(9) 1296.17 +	DK Lac			
			O I(2) 1302.17 + Si II(3) 04.37	1303.4	5.05	12.42	O I(2) 02.17 + Si II(3) 04.37
1338.1	3.63	9.15	C II(1) 35.10	1357.2	(3.11)	(7.02)	?
1395.2	5.73	12.12	Si IV(1) 1393.75 + 1402.77	1530.5	3.60	5.855	Si II(2) 1526.71
Q Cyg				HR Lyr			
1238.0	7.53	15.35	N V(1) 1238.82 + 1242.80	1243.4	5.00	7.92	N V(1) 1238.82 + 1242.80
1296.1	2.30	8.93	S I(9) 1296.17 +	1268.1	1.95	7.49	Si II(4)x3 1263 + Fe II (9) 60.54
			O I(2) 1302.17 + Si II(3) 04.37				+ S I x3 1270 ?
1384.6	6.61	16.45	S I 1385	1301.4	3.33	8.18	O I(2) 02.17 + Si II(3) 04.37
				1346.7	2.82	9.28	?
HR Del				1396.1	3.13	7.01	Si IV(1) 1393.75 + 1402.77
1259.8	1.35	9.43	Si II(4)x3 1263 + Fe II(9) 60.54				
			+S II(1) 59.52	GI Mon			
1303.1	1.01	7.12	O I(2) 02.17 + Si II (3) 04.37	1238.4	8.83	12.12	N V(1) 1238.82 + 1242.80
1367.5	1.85	12.45	N III(8) 70.20	1305.1	4.87	11.93	O I(2) 02.17 + Si II(3) 04.37
1390.1	1.12	7.45	Si IV(1) 1393.75 + 1402.77	1394.4	8.35	30.77	Si IV(1) 1393.75 + 1402.77
1535.9	6.16	17.85	C IV(1) 1550, P Cyg comp.	1372.2	4.16	12.02	N III(8) 70.20
				1541.1	4.15	12.25	C IV(1) 1548.18 + 1550.78
DN Gem							
1237.3	5.59	10.30	N V(1) 1238.82 + 1242.80	V841 Oph			
1300.9	1.41	8.43	O I(2) 02.17 + Si II (3) 04.37	1235.3	6.66	12.03	N V(1) 1238.82 + 1242.80
1379.2	3.65	15.84	N III(8) 70.20	1305.5	1.31	9.95	O I(2) 02.17 + Si II(3) 04.37
1541.4	1.90	6.40	C IV(1) 1548.18 + 1550.78	1372.0	1.64	8.46	N III(8) 70.20
V533 Her				RR Pic			
1240.1	3.43	9.92	N V(1) 1238.82 + 1242.80	1189.8	1.22	7.84	Si II 1190.42 (reseau ??)
1302.4	1.56	9.97	O I(2) 02.17 + Si II (3) 04.37	1202.2	1.14	6.73	N I 1200, Si II 1202
1336.2	1.53	14.35	C II(1) 35.10	1261.9	0.77	7.44	Si II(4) 60.42 + Fe II (9) 60.54
1374.2	2.72	13.46	N III(8) 70.20	1302.1	2.24	9.95	O I(2) 02.17 + Si II(3) 04.37
				1335.6	0.43	3.12	C II(1) 35.10
				1526.7	0.47	5.02	Si II(2) 26.70
				1609.7	0.49	6.75	Fe II (8) 08.80

Table 14. Wavelengths (Å), equivalent widths (Å), FWHM (Å), and identifications for the stellar absorption lines in FUSE and HST-STIS spectra.

λ_{obs}	*EW*	*FWHM*	Identification
T Aur			
1174.92	2.10	5.05	C III 1175.3
1238.27	3.16	7.70	N V(1) 1238.82 + 1242.80
1261.72	1.63	6.30	Si II(4) 60.42 + S II(1) 59.52
1300.08	5.85	11.87	O I(2) 02.17 + Si II(3)
1334.95	2.23	4.44	C II(1) 35.10
1392.23	1.08	3.93	Si IV(1) 1393.75 em. core
1402.09	1.86	7.73	Si IV(1) 1402.77 em. core
1502.29	1.23	5.60	?, see DI Lac
1525.86	1.19	5.01	Si II 1526.70
1532.90	2.36	9.94	Si II 1533.44
V533 Her			
1063.53	2.28	2.71	S IV 1062.7
1092.16	3.57	4.98	P IV 91.4 + 93.3 ?
1108.79	1.49	2.99	Si III 1108.4
1118.78	1.42	2.09	P V 1118.0
1122.95	0.92	2.59	Si IV 1122.5
1128.93	1.83	3.37	P V 1120.0 + Si IV 1128.3
1176.35	1.97	3.01	C III 1175.3
1183.62	2.20	3.48	N III 1183.0 ?
DI Lac			
1050.26	6.34	4.00	?
1064.01	9.73	7.41	S IV 1062.7
1077.90	5.66	2.81	S III (8) 77.1 ?
1092.36	3.62	2.51	P IV 91.4 + 93.3 ?
1235.60	7.08	11.61	N V(1) 1238.82 + 1242.80
1372.86	3.57	11.84	N III(8) 70.20
1502.96	1.02	5.03	?, see T Aur
1540.76	6.10	10.42	C IV(1) 1548.18 + 1550.78
RR Pic			
933.88	0.68	1.52	S VI 933.4
937.95	0.88	1.10	H I 937.8
944.87	0.96	2.88	S VI 944.5
950.05	1.53	2.62	H I 949.7
955.52	0.59	1.47	N IV 955.3
958.93	0.45	1.71	He II 958.7
997.72	0.52	1.83	Si III 997.4
1015.89	1.10	2.54	S III 1015.5
1021.12	0.64	1.82	Si II 1020.70
1062.86	0.85	1.79	S IV 1062.7
1073.31	0.73	1.56	S IV 1073.0
1113.39	0.46	1.50	Si III 1113.1
1118.17	0.95	1.84	P V 1118.0
1122.56	0.59	1.64	Si IV + Fe III 1122.5
1128.38	0.90	2.17	P V 1128.0 + Si IV 1128.3
1175.94	1.04	2.32	C III 1175
1183.43	1.60	3.74	?